Check for updates

A review of designable deep eutectic solvents for green fabrication of advanced functional materials

Zheng Wang,[a] Xinhui Zhao, [b] Yu Chen,[a] Cong Wei [*a] and Jingyun Jiang [*a]

Deep Eutectic Solvents (DESs) have become emerging green solvents within sustainable development and environmental protection. Characterized by their low toxicity, cost-effectiveness, environmental sustainability, and versatility, DESs are increasingly utilized across diverse sectors. Notably, in materials synthesis, these solvents offer the advantages of biodegradability and recyclability, bypassing high-temperature and high-pressure synthesis conditions, thus reducing environmental hazards and energy consumption while enhancing material performance. Consequently, adopting DESs as reactive or nonreactive media in nanomaterial synthesis has attracted significant attention. However, there are still knowledge gaps addressing the roles of DESs in developing and functionalizing advanced materials. This review regards these gaps by elucidating the unique chemical, thermal, and electrochemical properties of DESs. It then explores their recent applications in nanomaterial fabrication and discusses how DESs regulate material synthesis using three typical strategies, including chemical, thermal, and electrochemical processes. Additionally, it outlines the potential, key challenges, and limitations of using DESs in materials science. By providing a comprehensive analysis, this review aims to deepen understanding of DESs, broaden their use, and enhance their integration into materials synthesis practices.

Sustainability spotlight

With the rapid progress in green chemistry and clean energy, there is an increasing demand for scalable and sustainable methods to produce advanced energy materials. Deep eutectic solvents (DESs) are considered promising due to their low toxicity, affordability, environmental benefits, and versatility. However, while much research has explored their use in the synthesis and application of functional materials, the complex interactions between DESs and material structures remain insufficiently understood, limiting their effectiveness in guiding targeted material design. This demand for green fabrication aligns with the United Nations Sustainable Development Goals (SDGs), particularly Goal 7: Affordable and Clean Energy, and Goal 12: Responsible Consumption and Production. This review aims to advance scientific understanding, promote green energy innovations, support environmental stewardship, and inform policy development.

[a]School of Materials Science and Engineering, Zhengzhou University, Zhengzhou 450052, P. R. China. E-mail: weicong@zzu.edu.cn; jiangjingyun@zzu.edu.cn

[b]Jiangsu Key Laboratory of Function Control Technology for Advanced Materials, School of Environmental and Chemical Engineering, Jiangsu Ocean University, Lianyungang 222005, P. R. China

1 Introduction

The choice of solvent is a crucial topic in material synthesis, as the properties of the solvent can significantly impact the

Zheng Wang obtained her bachelor's degree from Huanghe Science and Technology College in 2023. He is currently pursuing a master's degree at Zhengzhou University, under the supervision of associate professor Jingyun Jiang and Cong Wei. His research interests include the design of novel eutectogel electrolytes and their impact on the performance of zinc-ion batteries.

Zheng Wang

Dr Xinhui Zhao received his PhD from Renmin University of China in 2020. He is currently a lecturer at Jiangsu Ocean University. His research focuses on deep Eutectic Solvents (DESs) and their applications. He has developed various DESs and used them for materials synthesis and biomass treatment.

Xinhui Zhao

feasibility of synthesis and the final material's properties. Among the approximately 600 existing volatile organic compounds widely used in research and industry, most are toxic and pose significant risks to both human health and the environment.[1,2] Over the past two decades, ionic liquids (ILs) have emerged as clean, efficient, and environmentally friendly alternatives to volatile organic solvents in various fields.[3] However, the limitations of ILs, such as toxicity, high cost, complex synthesis and purification processes, and non-renewability, are significant.[4] Therefore, pursuing safe, stable,

Yu Chen was born in 2000 in Henan Province, China. In 2023, he obtained his bachelor's degree from Henan University of Science and Technology. Under the guidance of associate professor Jingyun Jiang, he continues to pursue a master's degree at Zhengzhou University. His main research interest focuses on constructing eutectic electrolytes for zinc-ion batteries.

Yu Chen

Cong Wei received her PhD degree in Materials Science in 2016 from Chinese Academy of Sciences. He is currently an associate professor in the School of Materials Science and Engineering, University of Zhengzhou. His research interests include the design and synthesis of functional nanomaterials, two-dimensional nanomaterials and their applications in energy storage and sensors.

Cong Wei

Jingyun Jiang obtained her BS Degree in Chemistry from Henan Normal University in 2013 and PhD in Chemistry from Renmin University of China in 2018. After postdoctoral training, she joined the Zhengzhou University as an associate professor in the School of Materials Science and Engineering in 2021. Her research focuses on developing advanced function materials in the designable eutectic systems for efficient energy conversation and storage.

Jingyun Jiang

efficient, and sustainable solvents has become critical in fundamental research and practical applications.

Deep Eutectic Solvents (DESs) share several solvent properties with ILs, including low vapor pressure, high thermal stability, non-flammability, and ease of recovery. Unlike ILs, which are entirely ionic, DESs are primarily composed of molecular components, often in dominant proportions.[5] Due to their lower toxicity, reduced cost, simplicity in preparation, and broader solute applicability, DESs are increasingly regarded as environmentally favorable alternatives to ILs used in various applications.[6,7] The concept of DES was introduced in 2003 by Abbott *et al.* to address low melting points in mixtures. The 1ChCl–2urea DES, exemplifies this, maintaining a liquid state at room temperature with a melting point of only 12 °C, significantly lower than those of its separate components.[8] Typically, DES comprises combinations of hydrogen bond acceptors (HBAs) and hydrogen bond donors (HBDs), forming complex supramolecular structures through extensive hydrogen bonding, which significantly lowers the melting point by altering the free energy of the solid phase.[9] DESs' deviations from ideality are a result of their intrinsically cooperative intermolecular interactions, making them distinctly different from conventional ideal liquid mixtures. These features contribute to their unique properties, enabling their application in diverse fields such as catalysis, material synthesis, and electrochemistry. Abbott *et al.* classified the reported DESs into four types based on their components: type I (quaternary ammonium salts with metal chlorides), type II (quaternary ammonium salts with metal chloride hydrates), type III (quaternary ammonium salts with HBDs), and type IV (metal chloride hydrates with HBDs).[10] Moreover, non-ionic systems like thymol–lidocaine, which also remain liquid at room temperature, demonstrate a negative deviation from ideality across a broad composition range, leading to their consideration as type V DESs.[11] Despite these classifications, the categorization of DESs remains imperfect, with some systems involving Brønsted–Lowry acids and bases eluding conventional classification, highlighting the need for further refinement.[12]

Due to the diversity of DESs, they present significant advantages as reaction solvents in material synthesis. Firstly, they exhibit high solubility for diverse organic and inorganic precursors, facilitating uniform dispersion due to their polarity, hydrophilicity, and adaptability to various molecular sizes.[13] Secondly, the tunability of DESs allows precise nanoscale adjustments of composition, molar ratios, and water content, enabling control over the size and shape of metal nanoparticles and, consequently, the properties of the synthesized materials.[14] Thirdly, DESs fulfill multifunctional roles in synthesis, functioning as templates, directing agents, redox agents, stabilizers, or pH regulators, thereby preventing the need for additional reactants.[15] Fourthly, their low surface tension diminishes nucleation barriers, facilitating the formation of smaller particles.[16] However, the correlation between the properties of DESs and structures of target advanced materials is still vague, falling short of regulating the design paths towards high-performance materials. Therefore, it is necessary to advance the understanding of the chemical/thermal/electrochemical
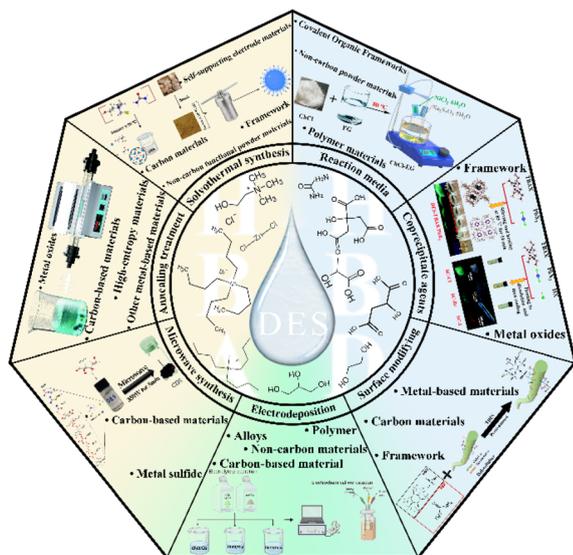
Fig. 1 The applications of DESs for advanced functional materials synthesis.

properties of DESs and depict their mechanism in material synthesis.

This review highlights recent progress in using DESs for materials synthesis, effectively linking their unique properties to the functionalization of advanced materials (Fig. 1). Initially, it discusses how the thermal properties of DESs control the formation of advanced materials through solvothermal, annealing, and microthermal techniques. Subsequently, the review addresses chemical strategies to synthesize advanced materials and illustrates how the chemical properties of DESs influence the structures of these materials. It also details the electrochemical properties of DESs and their mechanisms in the electrodeposition of functional materials. Utilizing the intrinsic properties of DESs, this review methodically examines their role in tailoring the functional properties of materials across various synthesis processes. As a comprehensive resource, this document supports green chemistry proponents and professionals in developing environmentally friendly and effective synthesis methods. Moreover, it delves into the versatile roles of DESs in materials science, evaluating their impact on material properties and highlighting the continual need for innovation.

2 Heat treatment

Heat treatment is a widely employed process in nanomaterials engineering that adjusts the crystal structure, grain size, and physical properties of materials through specific heating temperatures and cooling durations. Additionally, the composition and molar ratios of DESs are crucial in determining their thermal properties, significantly influencing the target materials' phase, morphology, and structure. The techniques utilized for heat treatment include solvothermal, annealing, and microwave synthesis, each distinguished by its unique experimental procedures.

2.1 Solvothermal synthesis

Solvothermal synthesis involves mixing reactants with DES, heating in autoclaves, cooling, solidifying, and washing away non-reactive DESs to obtain nanomaterials. This process typically requires no additional solvents or catalysts. The strong hydrogen bonding in DESs increases precursor solubility, making them suitable for various nanostructures. Due to their unique microstructure, DESs often act as templates and structure-directing agents. The reported materials include inorganic/organic frameworks, carbon materials, non-carbon powder materials, and self-supporting electrodes.

2.1.1 Organic–inorganic framework materials. Using DESs in solvothermal treatments, both metal–organic frameworks (MOFs) and zeolitic imidazolate frameworks (ZIFs) were synthesized. The synthesis parameters, including composition of the DES, concentrations of ligands and metals, reaction temperature, and duration, significantly influence the outcomes. Modifications to the HBDs within the DES composition are crucial, as they can modify the crystallinity of MOFs. For instance, MOFs synthesized in 1ChCl–2urea DES exhibit microcrystalline properties, while those produced in choline chloride–ethylene urea (e-urea) under the same conditions show a range of crystalline structures.[17] The phase of MOFs in 1ChCl–2urea can also be regulated by adjusting the metal/ligand molar ratio. DES acts as both solvent and structure-directing agent, inducing phase transitions from $Cu_3(BTC)_2$ (BTC = 1,3,5-benzenetricarboxylate) MOF to non-porous chloride-incorporating crystalline $Cu_2(BTC)Cl$ when heated, stabilized by halogen–metal bonds.[18] Heating a mixture of $TbCl_3 \cdot 6H_2O$, btbH$_3$, and NaOH in D-, L-, or DL-proline:7 thymol DES results in the synthesis of MIL-103 MOFs (btb = 1,3,5-benzenetrisbenzoate). A negative Cotton effect is observed in the MOF synthesized using an L-proline-based DES. In contrast, a positive effect emerges with D-proline, underscoring the impact of chiral DESs on the enantioenrichment of MOFs.[19] Wang *et al.* synthesized ZIF-67 hollow microspheres (ZIF-67-HMS) in 1ChCl–2urea using 2-methylimidazole and $Co(NO_3)_2 \cdot 6H_2O$. Compared to traditional organic solvents like methanol or ethanol, the synthesized ZIF-67 offers significant advantages such as regular morphology, good dispersibility, and a large specific surface area.[20]

2.1.2 Heteroatom-doped carbon materials. Deep solvothermal synthesis is also a versatile method for producing carbon materials, such as carbon dots, nanotubes, and support composites, with optional doping. In DES systems, doping elements are efficiently incorporated, as these solvents dissolve and serve as direct precursors for doped materials. Ren *et al.* used this technique to synthesize near-infrared fluorescent carbon quantum dots (PEG-CQDs) by mixing phenylenediamine (PPD)–polyethylene glycol 400 (PEG 400) DES with anhydrous ethanol.[21] Nitrogen-rich carbon quantum dots (N-CQDs) were prepared by combining 4-amino-4H-1,2,4-triazole-glycerol DES with anhydrous ethanol, which was further employed to detect Cr^{6+} in industrial wastewater, demonstrating excellent fluorescence stability.[22] N, Cl-doped carbon dots (N, Cl-CDs) were synthesized from longan shells using 1ChCl–2urea, which

served as the solvent and dopant. These N, Cl-CDs demonstrated robust redox sensing capabilities for MnO_4^-, Fe^{3+}, Cr^{6+}, and H_2O_2.[23] P-Doped CDs (P-DESCDs), with an average size of 3.15 nm, were synthesized using ChCl–lactic acid (LA) DES and H_3PO_4 as the phosphorus source. These P-DESCDs were subsequently grafted onto silicon surfaces using (3-aminopropyl)trimethoxysilane, forming a mixed-mode stationary phase, exhibiting improved separation performance and hydrophilicity.[24]

Beyond carbon dots, more extensive carbon materials are synthesized through a direct solvothermal process using DES. Lai *et al.* prepared solvothermal carbon (STC) using ChCl–citric acid (CA) DES and cotton stalk. Compared to hydrothermal carbon produced in water, the STCs exhibited higher carbonization and more significant amounts of carboxyl and phenolic groups.[25] The ChCl–CA system can also be applied to obtain $CoAl_2O_4/CNF$, which exhibited enhanced electrochemical performance as a battery-type electrode. The charge storage capacity of $CoAl_2O_4/CNFs$ is 2.2 times higher than that of $CoAl_2O_4$.[26] N-Doped carbon nanotubes (N-CNTs), which were synthesized using an acidified CNTs-ChCl–urea system. These N-CNTs effectively support the uniform dispersion of Pt nanoparticles. Theoretical calculations indicate that the d-band center of Pt in Pt/N-CNTs is near its Fermi energy level, exhibiting superior stability during the methanol oxidation reaction (MOR).[27] $PtSn_x/CNTs$ were synthesized using acetamide–[BMim]Br DES, where the Pt_3Sn intermetallic compound modulates Pt's geometric and electronic structures, enhancing hydrogen molecule activation.[28]

2.1.3 Non-carbon powder materials. Due to the superior dissolving capability of DESs, these solvents are employed to synthesize functionalized non-carbon powder materials by dissolving various metal precursors. Research has shown that mono- or binary metal oxides can be synthesized using ChCl-based DESs, where variations in components and their ratios significantly influence the structural properties of the oxide materials. Shahi *et al.* demonstrated synthesizing two distinct ZnO types with targeted exposure of the [0001] facet by adjusting the HBDs in DESs. In 1ChCl–2EG, ZnO with a petal-aggregated flower-like morphology was produced, whereas a cauliflower-like morphology was achieved using ChCl–CA DES, which notably enhanced the exposure of active sites and subsequently improved the efficiency of pollutant degradation.[29] 1ChCl–2urea DES also showed significant potential for fabricating binary metal oxides. Yao *et al.* prepared porous hexagonal $Co_2V_2O_7$ nanosheets by dissolving NH_4VO_3 and $CoCl_2 \cdot 6H_2O$ in 1ChCl–2urea DES. The amount of DES influenced the synthesis: 6 vol% resulted in uneven hexagonal morphology, while 26 vol% caused aggregation and edge fracture of the nanosheets. This is attributed to increased viscosity at higher DES concentrations, which hinders the growth of hexagonal nanosheets.[30] Coral leaf-like $MnMoO_4$ nanosheets with high surface area are prepared by adding $(CH_3CO_2)_2\cdot Mn\cdot4H_2O$ and $Na_2MoO_4\cdot2H_2O$ to 1ChCl–2urea DES.[31]

Thiourea (TU) is widely used as a sulfur source to stabilize the M–S bonds during the fabrication of metal sulfides. TU-based DES is often utilized as an ideal medium for synthesizing these
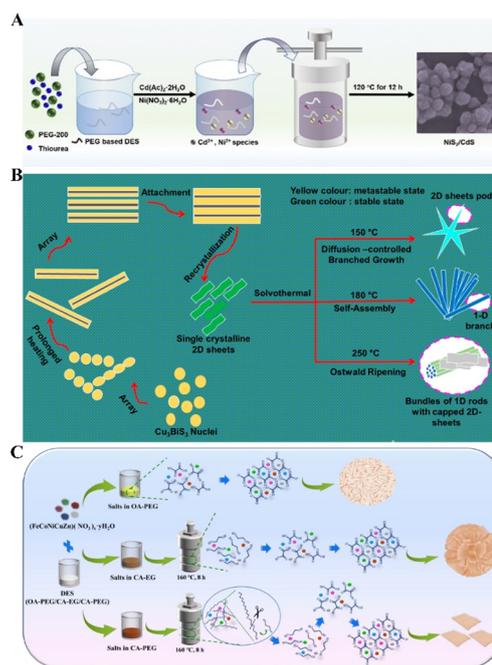

Fig. 2 Fabrication of non-carbon powder materials: (A) schematic illustration of NiS_2/CdS. Reprinted with permission from copyright© Wiley library, 2020.[32]. (B) Schematic illustration for plausible growth mechanism of CBS-1, CBS-2, and CBS-3. Reprinted with permission from copyright©American Chemical Society, 2021.[35]. (C) Schematic illustration of the synthetic process of $(FeCoNiCuZn)(C_2O_4)\cdot2H_2O$. Reprinted with permission from copyright© Elsevier Ltd, 2022.[37]

materials. For instance, Liu *et al.* synthesized a highly effective and bifunctional photocatalyst NiS_2/CdS nanospheres in the 2PEG 200–1TU DES (Fig. 2A). In this process, TU decomposes at elevated temperatures, reacting with Cd^{2+} and Ni^{2+} to form metal sulfides.[32] A similar situation was observed in Fe-doped NiS_2 systems, where varying the Fe to Ni ratio in PEG–TU affected the related electrocatalytic oxygen evolution reaction (OER) performance.[33] Other S-involved DESs, including ChCl–2thioacetamide, ChCl–2TU, and metal salt–TU, have also been employed to synthesize metal sulfides. For example, Zhang *et al.* utilized the 1ChCl–2thioacetamide DES to synthesize a range of metal sulfide nanocrystals, such as Sb_2S_3, Bi_2S_3, PbS, CuS, Ag_2S, ZnS, and CdS. This DES functions as a polar capping agent, stabilizing nanoparticles through electrostatic interactions, which prevents further growth or aggregation and lowers nucleation barriers, thereby aiding in forming smaller particles. Additionally, varying the reaction temperature and the molar ratio of ChCl to thioacetamide can modify the size and morphology of the crystals.[34] A similar temperature regulation was observed in the solvothermal synthesis of Cu_3BiS_3 (CBS) with 1D, 2D, and 1D–2D morphologies in the ChCl–TU DES at temperatures of 150, 180, and 250 °C, respectively (Fig. 2B). The ChCl–TU DES effectively combines the reactants through a restructuring effect induced by coordinative bonding and hydrogen bonding, resulting in different Cu_3BiS_3 morphologies.[35]

Some metal hydroxides and high-entropy oxalates can also be synthesized in DESs *via* solvothermal synthesis. Mo_2C,

$Ni(NO_3)_2 \cdot 6H_2O$, $Fe(NO_3)_3 \cdot 6H_2O$, and NH_4F were dissolved in 1ChCl–2urea to produce a novel NiFe-layered double hydroxide (LDH)/MoC nanocomposite through the solvothermal process. The multiple nanosheets' interconnected structure provides a smooth surface and a large specific surface area.[36] $Fe(NO_3)_3 \cdot 9H_2O$, $Co(NO_3)_2 \cdot 6H_2O$, $Ni(NO_3)_2 \cdot 6H_2O$, $Cu(NO_3)_2 \cdot 3H_2O$, and $Zn(NO_3)_2 \cdot 4H_2O$ were incorporated into PEG–CA and EG–CA DESs, leading to the formation of a single-phase multi-metal oxalate $(FeCoNiCuZn)(C_2O_4) \cdot 2H_2O$ (Fig. 2C). The DES's composition and structure critically influence the nucleation and growth of multi-metal oxalate salts. Notably, PEG supports the formation of 2D structures, whereas the lower molecular weight EG promotes the formation of 3D nanoparticles.[37]

2.1.4 Self-supporting electrode materials. A series of PEG-based DESs were designed and used for materials synthesis.[38] The dual-OH groups in PEG 200 can selectively adsorb onto certain surfaces to increase the growth rate, which can further effectively control the shape of the formed nanomaterials. Additionally, PEG-based DESs can be a non-ionic surfactant during preparation, exhibiting unique interaction with carbon collectors (Fig. 3A). PEG 200 and barbituric acid (BA) have migration activation barriers of 0.82 eV and 0.62 eV, respectively, indicating they can easily penetrate the graphite layers (Fig. 3B). Based on this conception, 2D non-van der Waals nanosheet-based self-supporting electrodes were obtained in PEG–BA DES confined carbon paper systems. Firstly, 2D spinel oxides with an average thickness of 3.4 nm were fabricated in the proposed PEG–BA–carbon paper systems (Fig. 3C). Introducing Ni onto the preassembled Fe–O–Co bimetallic active

sites, the oxidation states of Fe^{2+} and Co^{2+} were optimized, facilitating slight polaron hopping of valence electrons and further activating the Fe–O–Co sites.[39] Furthermore, by varying the molar ratio of the dissolved Ni/Fe salts, a self-supporting 2D $NiFe_2O_4/Ni(OH)_2$ heterostructure electrode was obtained. The strong electronic interactions between the $Ni(OH)_2$ and $NiFe_2O_4$ promote the formation of crystalline–amorphous co-existing catalytic active NiOOH, enhancing the interfacial reactivity of the heterostructure catalyst with the electrolyte.[40] Due to the excellent hydrogen bonding ability of chloride ions, metal chlorides were utilized to form the ternary and quandary DESs, such as PEG 200–BA-hydrated metal chloride ($MCl_2 \cdot xH_2O$) DESs (M = Fe, Co, Ni). The 2D amorphous bimetallic NiFe nitride (2DNiFe-N) grows between the graphite layers of CP. The ratio of Ni salt to Fe salt in the DES can be adjusted to control the Ni/Fe ratio in the metal nitride.[41] Additionally, the introduction of Cl^- modulates the electronic structure of 2D NiFe-N and controls dynamic self-reconstruction.[42] The prepared PEG 200–BA DES was also applied to synthesize 2D $CoNC@Co_2N$ heterostructures (Fig. 3D). Due to the properties of 2D non-van der Waals nanosheets and the formation of solid and conductive connections among CoNC nanosheets and CPs, the resulting 2D $CoNC@Co_2N$ exhibits superior OER and HER activities.[43]

Low-crystalline carbon cloth (CC) collectors were also applied in the DESs to fabricate self-supporting electrodes. For example, $NiCl_2 \cdot 6H_2O$–$CoCl_2 \cdot 6H_2O$–TU DES were introduced into an autoclave containing CC substrates to fabricate $CoNi_2S_4$/CC electrodes. Due to the DES's intense adhesion and liquid characteristics, $CoNi_2S_4$ nanosheets were uniformly deposited onto the CC substrate. The coupling of the two components enhanced electron transfer efficiency, preventing catalyst aggregation and corrosion during catalysis.[44] Metal foams, including Ni and Fe foam, are also ideal substrates to further react with DES to obtain self-supporting electrodes. Bifunctional Ni–Fe–P catalysts *in situ* grown on FF (Ni–Fe–P/FF) electrode were developed in the 1ChCl–2EG containing $NiCl_2 \cdot 6H_2O$, NaH_2PO_2, and $FeCl_3 \cdot 6H_2O$ systems. DES's unique solvent environment and the regulatory influence of Fe promote the formation of composition-controlled Ni–Fe–P.[45]

This chapter examines synthesizing diverse materials with substantial application potential using the solvothermal method in DESs. The materials produced encompass various frameworks, carbon-based substances, non-carbon powders (including metal oxides, sulfides, hydroxides, and oxalates), and self-supporting electrodes utilized across energy storage, catalysis, adsorption separation, sensing, and other fields. The solvothermal method with DESs allows for controlled morphology and structure, ensures high purity and excellent crystalline quality, and supports environmental sustainability.
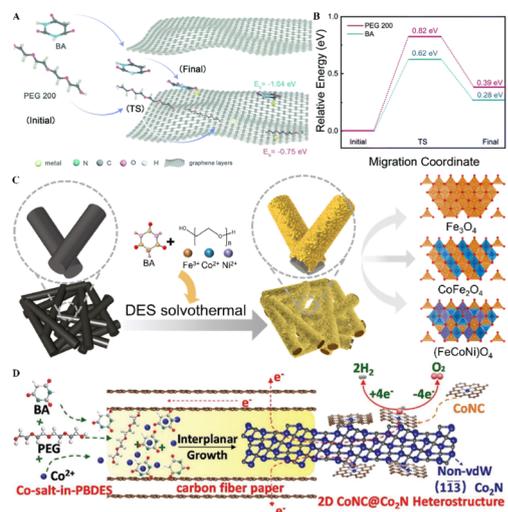

Fig. 3 Fabrication of self-supporting electrodes. (A) Schematic illustrating the migration path of BA and PEG 200 entering the graphitic layers and the corresponding binding energy. (B) Migration energy diagram of BA and PEG 200 entering the graphitic layers. Reprinted with permission from copyright© Royal Society of Chemistry, 2021.[39]. (C) Schematic illustration of the universal preparation of 2D spinel oxides. Reprinted with permission from copyright© Elsevier Ltd, 2022.[41]. (D) Schematic illustration of the fabrication process of 2D $CoNC@Co_2N$ heterostructures for water splitting. Reprinted with permission from copyright© Wiley-VCH GmbH, 2020.[43]

2.2 Annealing treatment

Annealing is a heat treatment process that occurs at higher temperatures than solvothermal. During annealing, components in DESs can decompose, producing bubbles that create pores and increase the surface area of the resulting materials. Additionally, DESs can serve as reactants, providing C or N/O/B/

S/P sources for fabricating advanced carbon materials. The proportions of components in DESs and the calcination temperature significantly impact the structure and properties of the resulting materials.

2.2.1 Highly porous carbon materials. In fabricating carbon materials, DESs function effectively as solvent mediums, facilitating the homogenization of diverse reagents such as biomass, coal, and polymers. Moreover, DESs can participate as reactants, incorporating elements like N, O, B, and S into carbon materials. This incorporation occurs through decomposition at elevated temperatures, enhancing the carbon materials' specific surface area and porosity. Furthermore, DESs that contain organic compounds can be employed directly as carbon sources in preparing carbon materials.

Firstly, biomass materials can be directly carbonized in DESs or pre-treated with DESs before carbonization. For example, Zou et al. dissolved bagasse in a DES containing $ZnCl_2$, urea, and varying ratios of KCl to synthesize nitrogen-rich porous carbon (NDPC) through one-step calcination (Fig. 4A). The DES served as a nitrogen source and activator, promoting the formation of the porous structure. Increasing the amount of KCl in the DES led to higher nitrogen doping content, specific surface area, and total pore volume.[46] Coconut shell can be dissolved in the $FeCl_3 \cdot 6H_2O$–urea–$NH_4HB_4O_7 \cdot 3H_2O$ DES and then calcined to obtain N/B co-doped porous carbon (NBPCs). The DES acts as an activating agent and a source of N/B, further decomposing to produce NH_3, H_2O, and B_2O_3 at high temperatures, which leads to numerous pores on the surface of the carbon material.[47]

A two-step annealing treatment can enhance the structural properties of carbon materials. Pre-treating biomass in DESs initiates pre-carbonization through solvothermal or microwave processes, which is advantageous over direct calcination. Furthermore, a broader range of biomass types can be employed. For example, Huang et al. employed a 2ChCl–formic acid DES to solvothermal dry microalgal powder's pre-carbonization. Following this, KOH activation produced N, O dual-doped ultra-microporous carbon. This process leveraged the DES to enhance the Maillard reaction, promoting the incorporation of nitrogen and oxygen into the carbon structure while minimizing their loss during chemical activation.[48] Amorphous activated carbon (AC) was obtained by calcinating the extracted lignin from the 1ChCl–9LA DES, resulting in large surface areas with micropores and mesopores.[49] Furthermore, Xu et al. utilized a 1ChCl–10LA DES to extract lignin from wheat straw. Extending the duration of processing increased lignin extraction at lower temperatures, whereas elevating the DES-to-biomass mass ratio enhanced the extraction efficiency at higher temperatures. The extracted lignin underwent activation via calcination with KOH, resulting in a hierarchical porous structure comprising both micropores and mesopores and achieved a significant specific surface area of 3577.3 m^2 g^{-1}.[50]

Secondly, coal serves as a precursor for O/N-doped hierarchical porous carbon (HPC) via a process that combines electrospinning and calcination. Initially, coal tar pitch mixed with a ChCl–phenol DES forms a fishnet-like structure through electrospinning, where the high viscosity of the DES enhances pitch spinnability while also supplying nitrogen. Subsequent calcination with $K_3C_6H_5O_7$ activates the carbon structure, creating a range of pore sizes, including significant micro- and ultramicropores (Fig. 4B).[51] In a separate process, Naomaohu coal undergoes microwave-assisted swelling with $FeCl_3$–levulinic acid DES, which disrupts chemical bonds and expands aromatic interlayer spacing. This swelling is followed by high-temperature pyrolysis, where Fe and Fe_2O_3 composites facilitate bond cleavage and enhance redox reactions, converting solid products into liquid and gaseous forms.[52]

Thirdly, DESs demonstrate significant solubility for biomass, coal, and polymers. ACs were synthesized from polyethylene terephthalate (PET) using 1ChCl–2urea via a two-step pyrolysis process (ITP2). This method involves pre-carbonizing PET at low temperatures within the DES, followed by high-temperature annealing. This approach minimizes PET decomposition, allowing the 2D crystal structure to develop progressively along the a and c axes. The resulting PET-CU-A-ITP2 samples exhibited a uniform elemental distribution, high graphitization, and substantial nitrogen doping.[53]

Fourthly, DESs can directly serve as a carbon source for synthesizing carbon materials. The composition, comprising HBAs, HBDs, and their respective molar ratios, significantly shapes the morphology and structure of the resultant materials. For instance, Zhou et al. utilized a calcination method on glucose–urea DESs at different molar ratios (7 : 3, 5 : 5, 3 : 7) to produce nitrogen-doped carbon nanosheets. In this synthesis, glucose polymerizes to form a three-dimensional carbon framework. At the same time, urea, acting as a nitrogen source and blowing agent, decomposes to release ammonia, enhancing pore formation and nitrogen incorporation. Adjusting the glucose-to-urea ratio allows for control over the pore structure and nitrogen content, and substituting urea with thiourea facilitates simultaneous doping of sulfur.[54]

The versatility of DESs facilitates the efficient synthesis of heteroatom-doped nanocomposites. These carbon materials, enhanced with heteroatoms, serve as ideal substrates for
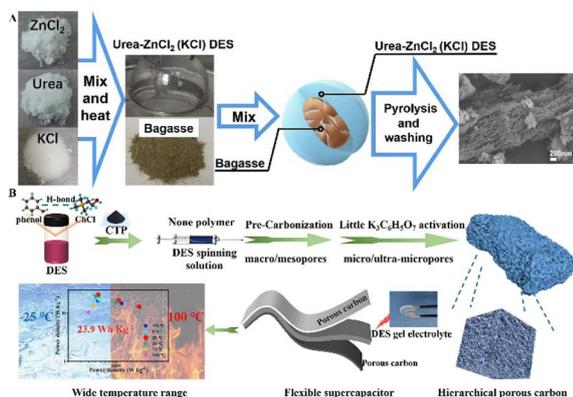

Fig. 4 Fabrication of carbon materials through the DES annealing process. (A) Schematic illustration of the procedures of the synthesis of DES and NDPC. Reprinted with permission from copyright© Elsevier Ltd, 2020.[46] (B) The schematic drawing for the preparation and application of CPCs. Reprinted with permission from copyright© Elsevier B.V, 2023.[51]

anchoring metal-based catalysts and promote the *in situ* formation of composites containing metals, metal nitrides, metal (hydro)oxides, and metal sulfides. For example, a $Co(NO_3)_2 \cdot 6H_2O$–ChCl–urea–glucose acid DES was employed to synthesize Co@N-doped porous carbon (Co@NPC), yielding a material with a hierarchical porous structure and an expanded surface area. Nitrogen doping varies during the synthesis, improving the interaction with transition metals and ensuring a uniform distribution of metal particles.[55] Another example involves the synthesis of ultrafine Co_4N nanodots anchored onto an N-doped carbon framework (Co_4N@NC) through calcination of a $CoCl_2$–malonic acid–urea DES. Here, malonic acid and urea decompose to form the framework, with Co_4N nanodots anchoring *via* hydrogen bonding, effectively preventing aggregation.[56] Mou *et al.* developed a g-C_3N_4/Fe_2O_3 nanocomposite by calcining a ternary urea–melamine–$FeCl_3$ DES. Adjusting DES ratios allows for controlled Fe_2O_3 loading, while the decomposition of organic components increases surface area and active site availability.[57] Similarly, MoN synthesized from a 1ChCl–2urea containing MoO_3, mixed with graphene aerogels (GA), forms a MoN@GA heterojunction that facilitates reduction and nitridation.[58] In a related study, Yang *et al.* used 1ChCl–2urea to disperse $H_2PtCl_6 \cdot 6H_2O$, $Ce(NO_3)_3$, and acid-treated MWCNTs evenly, producing Pt_2CeO_2/CNT heterojunction nanoclusters through calcination that enhanced the Pt(0) component, revealing more active sites at the Pt and CeO_2 interface.[59]

Metal sulfides@C composites can be synthesized *via* one-step or two-step annealing processes using DESs. Sulfur powder and thiourea are utilized as sulfide sources. For example, a mixture of sulfur powder and PEG–$SnCl_2 \cdot 2H_2O$ DES calcined produces sandwich-structured SnS@graphene composites, with SnS particles embedded between graphene layers. In this synthesis, DESs act as carbon sources and non-ionic surfactants, enhancing conductivity, reducing particle sizes, and preventing particle aggregation.[60] In addition, Co_9S_8@graphene (Co_9S_8@G) nanocomposites were created by thermal sulfidation of a $CoCl_2 \cdot 6H_2O$–PEG DES with sulfur powder at various temperatures, affecting the graphitization and morphology of Co_9S_8@G.[61] Furthermore, TU, another common sulfur source, was used in the synthesis of an In_2S_3/CdS/N-rGO hybrid photocatalyst through single-step calcination of a $CdCl_2 \cdot 2.5H_2O$–$InCl_3$–EG DES. This process ensures optimal integration of CdS/In_2S_3 with N-rGO, forming a cohesive interface and heterostructures with tremella-like morphology.[62] In another instance, 3D Co_9S_8@NSG (N/S-co-doped graphene) composites were produced through a one-step annealing of $CoCl_2 \cdot 6H_2O$–urea–thiourea–PEG DES. The heterojunction interfaces within these materials are finely adjustable by modifying the DES composition.[63] Zhang *et al.* synthesized Co_9S_8–Ni_3S_2@N, S, O-tri-doped carbon (NSOC) through one-step pyrolysis and sulfuration of a $NiCl_2 \cdot 6H_2O$/$CoCl_2 \cdot 6H_2O$–PEG 200–TU DES, with an increased proportion of Co altering the composite's phase behavior, diminishing the tubular Ni_3S_2 phase and enhancing the sheet-like Co_9S_8 structure.[64]

2.2.2 High-purity metal oxides with high surface areas. Metal oxides can be efficiently synthesized by annealing metals, metal oxides, or metal salts dissolved in DESs or using DESs composed of metal salts. This method operates under mild conditions and typically achieves high yields. During this process, the DES acts as a solvent and a reactant. Furthermore, the annealing temperature and the molar ratios of the reactants within the DES are critical in defining the structure and properties of the final products.

Firstly, a single metal can be dissolved in DESs to prepare the related functional metal oxides. Iwanow *et al.* prepared CuO by employing different DES compositions (glucose–urea and galactose–urea), using various copper precursors (Cu and CuO). The choice of DES influenced the grain size of Cu, particularly in the z-direction. Compact CuO nanoparticles around 100 nm were produced using Cu–DES systems, while copper oxide–DES systems yielded nanoparticles under 50 nm with larger pores and less ordered structures.[65] In another synthesis, mixing Sn and Se in 1ChCl–2urea formed the precursor $[(CH_3)_3N–(CH_2)_2-OH]_2[Sn_3Se_7] \cdot H_2O$, which was calcined to produce mesoporous SnO_2 (P-SnO_2). The DES facilitated hydrogen bonding, aiding material dissolution and promoting chemical reactions. Extending the calcination can increase the size and decrease the BET surface area of P-SnO_2.[66]

Secondly, DESs are particularly effective in dissolving metal oxides, thereby enabling their transformation into porous materials. For example, commercial Fe_3O_4 was dissolved in a ChCl–OA DES and exposed to microwave irradiation to produce Fe_3O_4 nanosheet precursors. These were subsequently calcined to generate porous Fe_3O_4 nanosheets (Fig. 5A).[67] Moreover, bimetallic oxides such as MFe_2O_4 (where M = Mg, Co, Ni, Zn) have been synthesized by dissolving Fe_2O_3 and another metal oxide in a ChCl–maleic acid DES, followed by a two-step calcination process (Fig. 5B). The exceptional solubility of metal oxides in DESs stems from the complex formation with these oxides rather than the disruption of metal-oxide bonds, allowing dissolution at significantly lower temperatures than traditional solid-phase reactions, thus reducing the energy
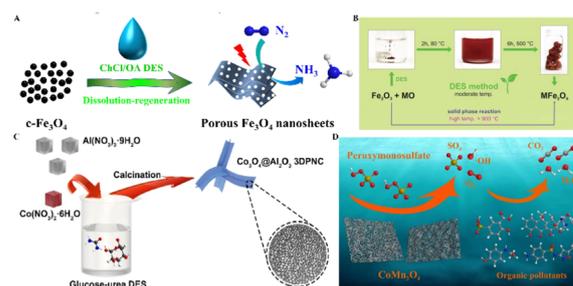

Fig. 5 Fabrication of metal oxides through the DES annealing process. (A) Schematic illustration for the synthesis process of porous Fe_3O_4-300 nanosheets. Reprinted with permission from copyright© Elsevier Inc, 2021.[67] (B) Schematic illustration for the synthesis process of MFe_2O_4. Reprinted with permission from copyright© WILEY-VCH Verlag GmbH, 2016.[68] (C) Schematic representation of the synthesis of Co_3O_4@Al_2O_3 3D PNC. Reprinted with permission from copyright© Tsinghua University Press, 2023.[74] (D) Schematic representation of HPNSs processing peroxydisulfate and organic pollutants. Reprinted with permission from copyright© Tsinghua University Press, 2023.[75]

required for synthesis.[68] A related study calcined a binary metal oxide-dissolved 1ChCl–2urea system to produce $M_2V_2O_{7-\delta}$ (M = Zn and Cu). During pyrolysis, ammonia released from urea decomposition helped stabilize oxygen vacancies and maintain reduced oxidation states within the metal oxide matrix.[69] Lastly, calcination of V_2O_5–$VOHPO_4 \cdot 0.5H_2O$ dissolved in a ChCl–glucose DES and a benzyl alcohol–isobutanol solution produced a vanadium phosphorus oxide (VPO) catalyst. In this process, the ChCl–glucose DES served as a structure-directing agent, facilitating the formation of active planes and resulting in highly crystalline precursors while concurrently reducing the acidity during calcination.[70]

Thirdly, inorganic and organic salts can be integrated into DESs to create metal oxides. For example, titanium butoxide (TBT), an organic salt, is soluble in ChCl–phenol DES and facilitates the synthesis of TiO_2 nanoparticles. As the calcination temperature rises, the nanoparticles' surface area and pore volume decrease due to pore collapse and disordered nanoparticle aggregation. Adjusting the ratio of TBT to DES allows for the control of TiO_2's exposed facets.[71] TiO_2 nanoparticles can be synthesized by combining tetra butyl titanate and tetrabutylammonium bromide–glycerol DES. The hydrogen bond network within the DES influences TiO_2's nucleation and growth by preferentially adsorbing on the nanoparticle surfaces.[72]

Inorganic salts are frequently employed to synthesize mono- or multi-metal oxides and their composites. Jaihindh et al. used varying molar ratios of 1ChCl–2urea and $Cu(NO_3)_3 \cdot 3H_2O$ aqueous solution to produce Cl-doped CuO. Acting as both a green solvent and a Cl-source, the DES facilitated the synthesis of CuO catalysts.[73] The $Co_3O_4@Al_2O_3$ 3D mesoporous nanocomposite was synthesized by calcining a glucose–urea DES containing $Al(NO_3)_3 \cdot 9H_2O$ and $Co(NO_3)_2 \cdot 6H_2O$ (Fig. 5C). This unique composite, featuring a hierarchical structure with open 3D helical microstructures and well-distributed Co_3O_4 particles, enhances active site accessibility and reduces mass transport distances.[74] Furthermore, $CoMn_2O_4$ hierarchical porous nanosheets (HPNSs) were synthesized through a microwave-assisted process involving preheating and calcination of $Co(NO_3)_2 \cdot 6H_2O$ and $Mn(NO_3)_2 \cdot 4H_2O$ dissolved in a glucose–urea DES (Fig. 5D). These nanosheets are characterized by their hierarchical porous structure.[75] Separately, Luke et al. synthesized honeycomb-layered $Na_3Ca_2BiO_6$ and orthorhombic $Na_3Ni_2BiO_6$ using a betaine–glucose DES, where DES decomposition at high temperatures facilitated the formation of porous structures.[76] Notably, $LaCl_3$ $NiCl_2$, $LaCl_3$, and $CoCl_2$ can dissolve in ChCl–malonic acid DES, in which a series of La-containing perovskite $LaTO_3$ (T = Mn, Mn/Ni, or Co) was achieved by a two-step calcining process. The DES enables the uniform mixing of metal precursors and facilitates the formation of the active intermediate LaOCl. The intermediate further reacts with binary metal oxides (Mn_3O_4, NiO, or Co_3O_4) to form their respective perovskites.[77]

Fourthly, direct calcinating metal salts-based DESs can also yield metal oxides, and adding surfactants during the calcination process can improve the materials' specific surface area and pore size distribution. For example, CeO_x nanoparticles were synthesized by calcining a $1Ce(NO_3)_3 \cdot 6H_2O$–3.5urea DES with various surfactants. Cationic surfactants, particularly those with longer chain lengths, increased porosity, and surface area more effectively than non-ionic types.[78] Additionally, $1SnCl_2$–2urea DES can mixed with tetraethyl orthosilicate to form a gel, which is then calcined to obtain SnO_2/SiO_2. Increasing the DES content in the sol–gel process reduces surface tension, shortens intermolecular colloidal interactions, and promotes the formation of smaller SiO_2 particles with greater surface area.[79]

High-entropy oxides (HEOs), composed of five or more metallic elements, have attracted considerable attention for their unique structures and properties, distinguishing them from conventional oxides. These HEOs can be synthesized using DESs through a two-stage process. For example, Guan et al. utilized DESs of PEG–TU, EG–CA, and EG–urea with $NiCl_2 \cdot 6H_2O$, $MnCl_2 \cdot 4H_2O$, $CoCl_2 \cdot 6H_2O$, $FeCl_3$, and $AlCl_3$, to synthesize diverse FeCuNiMnAl HEMs. By adjusting the composition and ratios of DESs, they achieved control over the morphology, influencing the metals' aggregation and structural form.[80] Additionally, a microwave pretreatment followed by calcination of $La(NO_3)_3 \cdot 6H_2O$, $Co(NO_3)_2 \cdot 6H_2O$, $Cr(NO_3)_3 \cdot 9H_2O$, $Fe(NO_3)_3 \cdot 9H_2O$, $Mn(NO_3)_2 \cdot 4H_2O$, and $Ni(NO_3)_2 \cdot 6H_2O$ in a glucose–urea DES facilitated the synthesis of $La(Co_{0.2}Cr_{0.2}Fe_{0.2}Mn_{0.2}Ni_{0.2})O_3$, alongside lithium- and sodium-doped variants. Including Li^+ and Na^+ improved surface oxygen vacancies and induced lattice distortions, resulting in finer grain sizes.[81] This glucose–urea DES also enabled the microwave-assisted synthesis of various 1D and 2D HEOs such as rock-salt (CoCuMgNiZn)O, spinel $(CoCrFeMnNi)_3O_4$, and perovskite $La(CoCrFeMeMiNi)O_3$. These HEOs exhibited uniform metal dispersion, substantial surface areas, and consistent single-phase structures enhanced by configurational entropy, making them suitable as negative electrode materials for LIBs.[82]

2.2.3 Other non-carbon materials. A bimetallic iron fluoride (BFF) comprising FeF_2 and FeF_3 phases is synthesized by calcining a mixture of $FeCl_2 \cdot 4H_2O$ and $CoCl_2 \cdot 6H_2O$, Ketjen black, and NH_4HF_2 in a ChCl–3EG DES. In this system, Co^{2+} acts as an oxidant, converting most Fe^{2+} into Fe^{3+}. This bimetallic composition combines the stability and narrow bandgap of FeF_2 with the higher capacity and potential of FeF_3, enhancing the cathode's cycling reversibility and capacity.[83] Oxygen-doped hexagonal-tungsten-bronze FeF_3 (FFH) was synthesized by calcining a Fe-based DES, comprising nitrite and methylsulfonylmethane with NH_4HF_2. This method offers a safer alternative by avoiding highly corrosive gases and the need for extreme reaction conditions. The fluorine's high electronegativity facilitates the disruption of Fe^{3+} interactions with O=S=O, favoring the formation of stable Fe–F bonds. Additionally, the selective presence of Fe^{3+} and Co^{2+} in the DES prevents the creation of cobalt fluoride compounds, transforming HTB-type FeF_3 into a 3D porous brick structure of interconnected nanoparticles.[84]

With the development of DES, more and more novel DESs were fabricated and utilized to prepare functional materials. Amino acid-based DESs demonstrate significant potential. Jiang et al. used a $FeCl_3 \cdot 6H_2O$–$CoCl_2 \cdot 6H_2O$–$NiCl_2 \cdot 6H_2O$–L-cysteine DES to synthesize hierarchical FeCoNi-based nitro-sulfide

(FeCoNi-NS), which uniformly incorporates N and S heteroatoms into Fe, Co, and N. This hierarchical porous structure enhances catalytic surface area and transport capability, which increases and diversifies active sites.[85] In another study, Wei et al. explored the effects of amino acid structure on metal reduction by synthesizing $Ni/Ni(OH)_2$ and metallic Ni from $NiCl_2\cdot 6H_2O$–serine $NiCl_2\cdot 6H_2O$–threonine DES, respectively. The presence of a methyl group in serine enhances its reduction capability, leading to complete reduction to metallic Ni, whereas threonine yields a unique ultrathin heterostructure of Ni (0) embedded in $Ni(OH)_2$ nanosheets.[86]

The calcination of DESs effectively promotes the formation of stable, porous structures, thereby increasing the specific surface area and enhancing performance in catalysis, adsorption, and other applications. Key aspects include: (i) DES' strong eutectic properties enable effective integration with reactants, producing uniformly distributed mixtures; (ii) DES decomposition facilitates pore creation and influences the structural transition from crystalline to amorphous forms; (iii) the multicomponent nature of DESs supports the multifunctionality of the resulting materials; (iv) the inherently low-toxic and environmentally friendly nature of DES components favors large-scale applications.

2.3 Microwave synthesis

Microwave synthesis, another one-pot process, involves directly loading all reagents into the microwave reactor. Unlike solvothermal and annealing, this method efficiently transmits energy via radiation interactions, significantly shortening reaction times. In this technique, DES precursors are uniformly and rapidly heated within microwave fields, capitalizing on conduction, polarization effects, and molecular interactions.

DESs can dissolve organic compounds and biomass, facilitating microwave-assisted synthesis of carbon materials. For instance, glucose dissolved in various ChCl-based DESs produces CDs, with the DESs acting as passivating agents, dopants, and solvents. Modifying DES components allows for the tailored adjustment of heteroatom doping levels. Shorter carbon chains in the DES and higher concentrations of functional groups (–NH2, –OH) improve quantum yields.[87] Kaur et al. processed powdered wheat straw with LA–ZnCl2 DES under microwave irradiation, converting it into oxidized graphitic material. This method includes using water to regenerate graphene, promoting DES recycling, and enhancing process sustainability.[88] Xie's microwave-assisted pretreatment of bamboo holocellulose in a ChCl–zinc acetate (ZAC) DES yielded fermentable sugars and nanocellulose, preserving equipment and improving sustainability by altering the crystalline and microstructure of cellulose.[89] Additionally, Adeyemi et al. synthesized $AgInS_2$ and other compounds, adjusting concentrations to control crystallinity and particle sizes, using a two-step heating profile for thorough dissolution and size control.[90,91] Therefore, microwave techniques in DES systems shorten reaction times, enhance yields, and allow precise control of material properties, though research in this area remains limited. Future studies should explore the potential of

DESs and microwave synthesis for creating functional materials, potentially revolutionizing material synthesis and applications.

Solvothermal synthesis, microwave synthesis, and calcination are pivotal thermal treatment methods for synthesizing materials using DESs. These techniques allow meticulous control over reaction conditions—temperature, duration, and DES composition—tailoring various functional materials' microstructure and macroscopic properties. Solvothermal synthesis involves heating precursors with DESs in a sealed vessel, typically at lower temperatures than calcination, ensuring superior control over reaction conditions and product purity. This method is ideal for temperature-sensitive materials such as MOFs, COFs, metal sulfides, and phosphides. Conversely, calcination subjects materials to high temperatures to promote transformation and crystallization, which is crucial for developing specific crystal structures in porous carbon materials and metal oxides. Microwave synthesis leverages microwave radiation to expedite reactions, offering rapid processing at lower temperatures, thus enhancing safety and reducing energy consumption. It ensures even heating, which may result in more uniformly structured materials. While all three methods are effective for material synthesis, their application varies depending on the specific needs and properties of the target products.

3 Precipitation synthesis

Precipitation synthesis is a technique for preparing nanomaterials under ambient pressure and temperature, significantly reducing energy requirements. In this method, DESs act predominantly as inert solvent media, simplifying their recovery and reuse. Furthermore, DESs can engage with various reactants, such as acids, bases, oxidizers, and reducers, to facilitate coprecipitation. This approach also enables modifying materials within DESs to improve their existing properties or impart new functionalities. DESs serve three primary functions in precipitation synthesis: reaction media, coprecipitation facilitators, and surface-modifying agents.

3.1 Reaction media

DESs, as green and economical reaction media, provide distinct advantages in precipitation synthesis. They facilitate reactions at lower temperatures than conventional methods, enabling efficient synthesis of desired products. DESs exhibit high solubility and diffusivity, ensuring uniform solute distribution and enhancing reaction efficiency and product purity. Additionally, their stability and recyclability contribute to minimal waste, aligning with the principles of green chemistry.

Combining covalent organic frameworks (COFs) using DESs significantly reduces energy consumption, shortens reaction times, and eliminates the need for hazardous solvents. The composition of DESs and the controlled reaction parameters, such as time and temperature, are crucial in determining the structural characteristics of COFs. Deng et al. demonstrated the high yield and crystallinity of imine-linked COFs synthesized using a ChCl–hexafluoroisopropanol (HFsIP) DES, which also
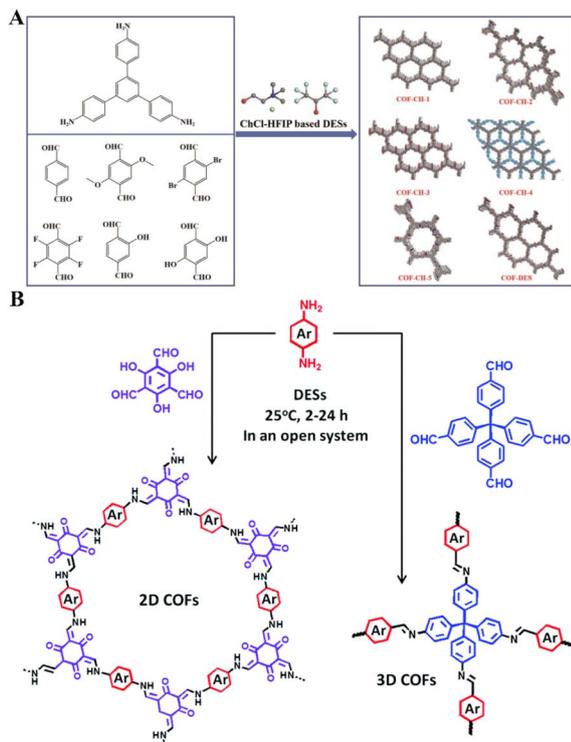
Fig. 6 Framework materials fabrication *via* precipitation, utilizing DESs as the reaction medium. (A) Preparation processes of the selected imine-linked COFs. Reprinted with permission from copyright© American Chemical Society, 2023.[92]. (B) Schematic illustration of the syntheses of 2D and 3D COFs. Reprinted with permission from copyright© Royal Society of Chemistry, 2020.[93]

acted as a catalyst (Fig. 6A). They observed that a DES ratio of 1ChCl–4HFIP produced the highest crystallinity in TPB-TPDD-based COFs. Variations in solubility and acidity among different DES compositions affect these outcomes, with reaction conditions further refining crystallinity.[92] Qiu *et al.* synthesized various 2D (keto-enamine, azine, and hydrazone-linked) and 3D imine-linked COFs using 1ChCl–2Gly, 1ChCl–2urea, 1ChCl–2EG DESs, achieving superior crystallinity and surface areas within 2 h at room temperature (Fig. 6B). Additionally, these DESs could be recycled up to three times with minimal loss in efficacy.[93] Ce–Fe Prussian blue analogs (Ce–Fe PBAs) were synthesized in the ChCl–CA DES containing $Ce(NO_3)_3 \cdot 6H_2O$, $K_3[Fe(CN)_6]$, water, and ethanol. The competitive complex of Ce^{3+}–citrate ions and Ce^{3+}–ferricyanide ions moderated the nucleation rate, yielding uniformly structured Ce–Fe PBAs. The crystallization of PBAs, influenced by the ethanol-to-water volume ratio and the molar ratio of DES to metal ions, dictated the morphology, dimensions, and chemical composition of the resultant Ce–Fe oxides following calcination.[94]

Chloride ions in DES significantly affect the reduction potential of noble metals, thereby enhancing their reduction rates. This makes ChCl-based DESs containing halide ions particularly effective for synthesizing noble metal nanomaterials. Kim *et al.* utilized 1ChCl–2acrylamide DES to produce a series of nanoparticles, including Au, Ag, Pd, Pd@Ag, and Au@Pd. In this process, acrylamide undergoes radical

polymerization upon heating, transitioning from liquid to solid phase. This change facilitates the stabilization of high concentrations of Au NPs and ensures their uniform dispersion.[95] Additionally, intermetallic PtPd nanocrystals were obtained in 1ChCl–2EG DES, in which the DES served dual roles as a reducing agent and shape-directing agent. This approach efficiently reduced Pt^{4+}/Pd^2 to PtPd nanocrystals within six minutes, producing octahedral nanoparticles.[96] Moreover, DESs can act purely as reaction media without participating directly in the reactions. For example, when added to a DES solution containing zinc complexes, EG induces desolvation, promoting the aggregation and growth of ZnO crystals along the *c*-axis. In cases where ZnO is dissolved in a 1ChCl–2urea DES, the addition of EG results in the precipitation of uniquely shaped double-cone ZnO mesocrystals.[97]

External agents such as reducing agent hydrazine ($N_2H_4 \cdot H_2O$), oxidizing agent ($Na_2S_2O_3 \cdot 5H_2O$), and alkali (KOH) can be combined with metal salts in DESs to synthesize metal oxides or sulfides. For instance, adding $N_2H_4 \cdot H_2O$ to a ChCl–D-lactic acid DES containing $ZnCl_2$ leads to the formation of rod-like and spherical ZnO nanoparticles.[98] Furthermore, introducing $N_2H_4 \cdot H_2O$ into 1ChCl–2urea or 1ChCl–2EG DES results in the synthesis of HgS, ZrO_2, MnO_2, and CuO nanoparticles, which range in size from 50 to 150 nm after a specified reaction time.[99] $Na_2S_2O_3 \cdot 5H_2O$ serves as both an oxidant and a sulfur source, facilitating the oxidation of $NiCl_2 \cdot 6H_2O$ into Ni_3S_4/NiS_2 composites within 1ChCl–2EG DES. The DES provides structural stability and functions as a solvent and a template during synthesis. Adjusting the concentrations of $NiCl_2 \cdot 6H_2O$ and $Na_2S_2O_3 \cdot 5H_2O$ yields various structural forms of Ni_3S_4/NiS_2, including wrinkled, lamellar, and layer-rolled morphologies.[100]

In polymerization, DESs often negate the need for additional initiators, simplifying the reaction setup, reducing costs, and enhancing controllability and repeatability. For instance, poly(furfuryl alcohol) (PFA) was polymerized from FA in ChCl–2ZnCl$_2$ DES, eliminating the need for external solvents or initiators (Fig. 7A). The polymerization efficiency of FA increased with higher reaction temperatures and DES/FA weight ratios. Moreover, the DESs proved recyclable, demonstrating their potential for sustainable and large-scale PFA production.[101] In another example, zwitterionic eutectogels were produced from acrylamide in various betaine (Bet)-based DESs, such as Bet–Gly, Bet–EG, and Bet–urea, facilitated by noncovalent interactions (Fig. 7B). The eutectogel from Bet–Gly DES exhibited superior properties, including an ion conductivity of 0.23 mS cm^{-1}, an elongation capability of 1400%, and a self-healing property of 82.01%. These features made the eutectogel ideal for wearable self-adhesive strain sensors, capable of adhering to skin and sensitively monitoring body movements over a wide temperature range.[102]

DESs offer numerous advantages as reaction media: they facilitate synthesis under mild conditions, increase solubility and stability, enable recyclability, and simplify the system. These characteristics make DESs highly promising for diverse applications, including synthesizing COFs, noble metal nanoparticles, metal oxides and sulfides, and polymers. Ongoing research is anticipated to highlight their importance as green solvents further.
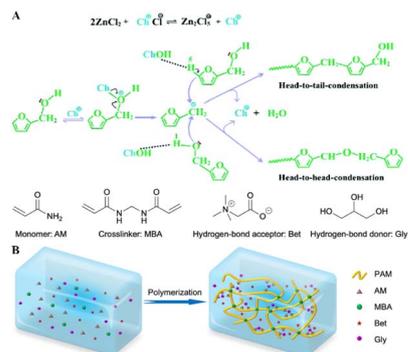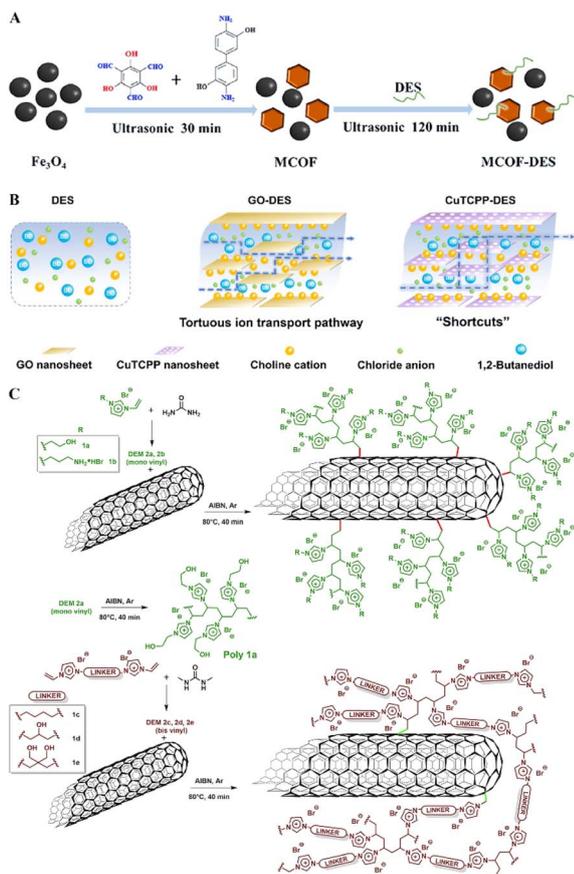
Fig. 9 Materials fabrication *via* precipitation, utilizing DESs as the surface modifying agents. (A) Synthesis process of MCOF-DES for the extraction of Cu^{2+}. Adapted with permission from copyright© Elsevier B.V., 2024.[108]. (B) Schematic illustration of DES, GO-DES, and CuTCPP-DES. Reprinted with permission from copyright© Royal Society of Chemistry, 2023.[110]. (C) Synthetic procedure for the preparation of DES-modified MWCNTs. Reprinted with permission from copyright© The Elsevier B.V., 2023.[113]

fire resistance, mechanical strength, and optical properties of the PHCNFs.[111] Similarly, graphite felt surfaces were modified using NH_4Cl–$FeCl_3$ or 1ChCl–2urea DES, enhancing the surface area by 46% and increasing disorder and defects within the graphite structure.[112] Valentino *et al.* introduced a novel subclass of polymerizable deep eutectic monomers (DEMs) consisting of mono- and bis-vinyl imidazolium salts equipped with various functional groups (–OH, –NH_2, –NH_3^+Br^-). These DEMs served as both a dispersing medium and a structure-directing agent, facilitating free radical-induced polymerization directly on the MWCNTs' surfaces, which also acted as templates to guide the orderly polymer network formation (Fig. 9C).[113]

In addition, various DES-modified metal compounds with abundant functional groups have been developed. Ahmad *et al.* used tetra butyl phosphonium bromide and various carboxylic acids (hexanoic, pentanoic, butyric, propanoic, acetic, and formic acid) in a phosphoryl DES to enhance the surface of cerium oxide nanoparticles (CeNPs), achieving high CO_2 adsorption at

low pressure.[114] Lauric acid-based DESs, combining lauric acid with capric acid, octoic acid, nonanoic acid, and thymol, were employed to modify $Cs_3Cu_2I_5$, creating sensitive NH_3 fluorescence sensors. These sensors effectively adsorb and react with NH_3 on their surface, drastically reducing fluorescence intensity due to interactions with the –COOH group in DES.[115] Furthermore, $Fe(CO)_5$ was processed in a TBAC–decanoic DES to produce TBAC acid DES@Fe, subsequently enhanced with N, S-doped amorphous carbon to create N, S-doped amorphous carbon/TBAC acid DES@Fe. This design inhibits particle aggregation and leverages π–π interactions for adsorption.[116]

This chapter delves into the multifaceted roles of DESs in synthesis, underscoring their effectiveness as reaction solvents, coprecipitation agents, and surface modifiers, all under environmentally benign conditions that adhere to the principles of green chemistry. Initially, we discuss the role of DESs as reaction media. Their distinctive properties enable the dissolution of a broad spectrum of chemical entities, thereby boosting reaction yields and facilitating the recovery of solvents post-reaction, which minimizes environmental footprint. Furthermore, DESs actively engage in the synthesis process as coprecipitation agents, forming materials such as ZIFs, metal oxides, and sulfides. Their capacity as reducing agents demonstrates remarkable flexibility, broadening their application in creating innovative materials. In their capacity as surface modifiers, DESs bolster the performance of MOFs and carbon materials by enhancing stability, conductivity, and adsorption capabilities. This versatile functionality highlights the pivotal role of DESs in pushing the boundaries of material science within eco-friendly frameworks, offering groundbreaking solutions for sustainable advancement.

4 Electrodeposition

DESs have gained prominence in electrodeposition due to their exceptional physicochemical properties. These solvents are characterized by low volatility, high solubility, and a wide operational temperature range, enabling efficient dissolution of metal precursors and providing excellent conductivity and a stable electrochemical window. In electrodeposition, DESs enable precise deposition of nanomaterials, including alloys and carbon-based materials. Strategic inclusion of additives during the process tailors material morphology and incorporates beneficial impurities to enhance the quality of the deposits. Additionally, the environmental sustainability and tunability of DESs support the green chemistry objectives of contemporary industries.

4.1 Precise composition control of alloys

ChCl-based DESs are extensively utilized in electrodeposition due to their superior ion conductivity, low viscosity, and excellent electrochemical stability. The composition of HBDs like urea, EG, and Gly significantly impacts the formation of metal complexes, influencing the structure of resultant metal alloys during electrolysis. Sales *et al.* demonstrated this by synthesizing Fe–Mn alloys using DESs composed of 1ChCl–2EG, ChCl–

Gly, or 1ChCl–2urea DES. Variations in coordination complexation between Mn^{2+} and the HBDs led to significant differences in manganese content and morphology of the alloys.[117] 1D tellurium (Te) rods, preferentially growing along the [001] axis from the (100) planes, were electrodeposited onto a gold surface using 1ChCl–2urea and 1ChCl–2EG DESs. In these systems, chloride ions and EG or urea coordinated with Te^{4+} to form complexes facilitating one-dimensional growth under sufficiently negative potentials. The viscosity of the DES impacted the diffusion coefficients of these complexes, thereby influencing the microtopography and diameter of the Te rods.[118]

Pd, Rh, and PdRh NPs were electrodeposited from 1ChCl–2urea DES containing respective metal chlorides, showcasing the adaptability of DESs in generating advanced materials with tailored properties.[119] Notably, a concave triple-octahedral Au–Pd alloy was deposited using 1ChCl–2urea DES, exemplifying the potential of DESs in fine-tuning material properties for specific applications.[120] Concave nanocubes of Pt-RE alloys (RE = La, Y, Sc) featuring high-index facets were also synthesized in DES, enhancing nitrogen reduction activity by strengthening the bond with reaction intermediates.[121] Additionally, porous Ni and Fe NPs were electrolytically deposited onto stainless steel mesh from a 1ChCl–2urea containing $NiCl_2$ and $FeCl_3$. The resultant NiFe@SS electrode demonstrated a significantly larger ECSA than Ni@SS alone, delivering enhanced OER performance.[122] $Ni(OH)_2$/Ni/carbon felt composite electrodes were also produced *via* single-step electrodeposition in a water-involved 1ChCl–2urea system. Water content influenced the crystal structures and morphologies: with 10% water, nanosheets were evenly distributed, whereas at 20% water, they began to clump into irregular clusters.[123]

1ChCl–2EG DES is also frequently utilized for the electrochemical deposition of alloys. The composition of these alloys is determined by the concentration of metal precursors in the DES. For instance, Pd and Sn were electrodeposited onto SS using 1ChCl–2EG DES containing $PdCl_2$ and $SnCl_2$, forming Pd–Sn/SS electrodes. These electrodes consistently achieved nitrate conversion rates exceeding 90%, demonstrating that the preparation method in the DES has a significant impact on nitrate reduction.[124] Deomar *et al.* used 1ChCl–2EG DES to dissolve Zn and Co salts for the electrodeposition of Zn, Co, and Zn–Co coatings. These DES-based electrolytes demonstrated high conductivity, abundant metal ions, resistance to high temperatures, and biodegradability. The atomic ratio of Zn to Co in the deposits accurately reflected their molar ratios in the electrolyte, highlighting DES's capability to dictate the composition of Zn–Co coatings precisely.[125] Further research in the 1ChCl–2EG DES led to the electrodeposition of ternary Zn–Sn–In coatings on 1020 carbon steel substrates, enhancing corrosion resistance. Increasing the concentration of In^{3+} refined the grain size and improved deposition efficiency, affecting current density and charge time.[126] Additionally, a Ni–Co–Zn alloy was pulse-electrodeposited from 1ChCl–2EG DES containing $ZnCl_2$, $CoCl_2$, and $NiCl_2$. The resulting alloy coating was uniformly dense with spherical particles.[127]

Ternary ChCl–EG–Gly DES containing $AgNO_3$ was applied to electrodeposit Ag and subjected to a galvanic replacement
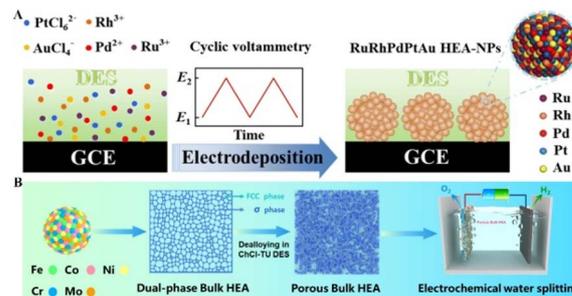

Fig. 10 Fabrication of HEOs through the DES electrodeposition process. (A) Illustration of the programmed electrodeposition method for the preparation of RuRhPdPtAu HEA-NPs. Reprinted with permission from copyright© Royal Society of Chemistry, 2023.[129]. (B) Process outline for electrochemical dealloying in ChCl–TU DES of FeCoNiCrMo HEA. Reprinted with permission from copyright© American Chemical Society, 2023.[130]

reaction with $PdCl_2$ and $HAuCl_4$ to fabricate a hollow dendritic Au/Pd/Ag electrode. The viscosity of the DES influences the transport rate of Pd^{2+} ions, affecting the speed of substitution reactions and the formation of the hollow structure. The duration of this substitution is critical in determining the electrode's morphology and composition.[128] RuRhPdPtAu NPs can be fabricated through electrodeposition from 1ChCl–2urea DES containing $RuCl_3$, $RhCl_3$, $PdCl_2$, K_2PtCl_6, and $HAuCl_3$ (Fig. 10A). These NPs form spherical aggregates characterized by extensive defects, providing high entropy and numerous active sites essential for their functionality.[129] Furthermore, FeCoNiCrMo is processed through electrochemical dealloying in a ChCl–TU DES, altering their surface and internal structures (Fig. 10B). This technique yields a 3D porous structure with particle diameters of approximately 100 nm, which optimizes the electronic configuration crucial for OER activity.[130]

4.2 Carbon-metal composites

Electrodeposition in DES electrolytes is an effective method for preparing and modifying carbon-metal materials. Liu *et al.* utilized a mixture of 1ChCl–2EG DES and ammonium chloride for pulse electrodeposition, producing amorphous carbon coatings (ACC) on 316L stainless steel. This technique facilitated strong carbon–iron bonding, significantly improving the substrate's corrosion resistance.[131] Similarly, a film of tin-reduced graphene oxide (Sn-rGO) was electrodeposited onto copper plates using 1ChCl–2EG DES solution containing tin(II) chloride and graphene oxide, ensuring even dispersion of graphene oxide and seamless integration into the tin matrix. The presence of rGO influenced the crystal growth direction of Sn, suppressing growth along the (101), (211), (301), and (112) planes and promoting it on the (200), (220), (400), (321), (420), and (501) planes, thereby enhancing the composite's corrosion resistance.[132] Furthermore, CNT has been modified effectively through electrodeposition. Employing a pulse reverse current electrochemical method in a ChCl–Gly DES containing CNTs enabled the deposition of Ag NPs, which significantly improved

specific capacitance and capacitance retention.[133] CNTs were templates for fabricating Ni/Sb co-doped TiO_2 electrodes via electrolysis in a 1ChCl–urea DES composed of $NiCl_2 \cdot 6H_2O$, $SbCl_3$, $SnCl_2 \cdot 2H_2O$, and CNTs. This electrode exhibited a rough surface, high coating hardness, and adhesion strength, a uniform coating structure, abundant adsorbed hydroxyl groups, enhanced active oxygen species presence, and improved charge transfer rates.[134]

4.3 Electropolymerized polymers

Specific polymer monomers are capable of undergoing electropolymerization in DESs. The polymers produced range from single-component polymers to composites, synthesized using binary DESs with or without additional water. Additionally, introducing acids into these DESs promotes polymerization.

1ChCl–2urea DES, for example, was used to electropolymerize poly(1,5-diaminonaphthalene) (PDAN) onto CC electrodes, yielding PDAN/CC composites. As electropolymerization progressed, PDAN's morphology evolved from granular to compact, enhancing its electrochemical charge storage capabilities due to its amine/imino groups' redox activities and electrolyte anions' (de)intercalation.[135] Pyrrole (Py) was electropolymerized in a ChCl–propionic acid DES with Fe_3O_4 NPs to produce a PPy/Fe_3O_4 nanocomposite, where the acid facilitated redox processes within the PPy membranes.[136] Pyrrole was also polymerized in a ChCl–LA DES, incorporating graphene sheets into the polymer matrix on a TiZr substrate, creating TiZr–PPy–GS. This composite, serving as an effective drug reservoir, showed enhanced hydrophilicity and improved antibacterial properties.[137] Melamine was electropolymerized onto MWCNT-modified GCE in 1ChCl–2EG DES, forming a PME/MWCNTs/GCE composite.[138] Additionally, polymethylene blue (PMB) and Au NPs were sequentially electropolymerized and deposited onto screen-printed carbon electrodes (SPCE) with zinc oxide nanorods in 1ChCl–2EG DES, enhancing the electrode's functionality.[139]

Acid doping in DES has been shown to boost polymer growth more effectively than undoped systems. For instance, phenazine was electropolymerized in acid-doped 1ChCl–2EG DES and deposited on a Fe_2O_3 NP-modified GCE, resulting in a nanostructured poly(phenazine)/Fe_2O_3 film compelling for hydrogen peroxide biosensing.[140] Furthermore, poly(cresyl violet) was electropolymerized on a CNT-modified GCE in 1ChCl–2EG DES mixture with acetic acid, where water enhanced the polymer's redox activity.[141] Another complex, poly(thionine-methylene blue) (PTH-MB), was formed in a ChCl–malic acid–water system on electrochemically reduced graphene oxide-modified GCE (ERG/GCE), displaying notable electrocatalytic activity towards nicotinamide adenine dinucleotide.[142] Similarly, poly-neutral red (PNR) was developed in an acid-doped ChCl–ethylene glycol–fructose DES on a CNT-modified GCE, showing improved electrochemical performance and selectivity for acetaminophen detection.[143] Hydrochloric acid (HCl) was incorporated to modulate the viscosity and improve the ionic conductivity of the ChCl–OA–EG DES, facilitating the formation of a robust polymethylene green (PMG) polymer.[144]

4.4 Non-carbon powder materials

Metal oxides, hydroxides, and phosphates can be electrodeposited from DES. For instance, γ-Fe_2O_3 is synthesized through two distinct methods: one involves electrolyzing iron anodes in 1ChCl–2urea either with[145] or without[146] phosphate. In the first method, iron atoms on the anode are oxidized to Fe^{3+}, while in the second method, Fe^{2+} in the electrolyte is electrochemically converted to Fe^{3+}. The resulting Fe^{3+} reacts with active oxygen produced during DES decomposition, forming iron oxide nanocrystals. Concurrently, amino group radicals generated from urea decomposition are grafted onto these particles, improving their dispersibility. Ni–Co–P films electrodeposited onto CC substrates from a methyl triphenyl-phosphonium bromide–EG DES display a surface rich in both amorphous and crystalline structures.[147] Similarly, Ni–Mo–P coatings are obtained by electrolyzing a complex system containing NaH_2PO_2, citric acid, ammonium molybdate, $NiCl_2$, and 1ChCl–2EG DES. The ionic nature of the DES promotes the formation of a rough Ni–Mo–P surface, providing abundant active sites for HER.[148] Additionally, a nanoporous Fe-doped $Ni(OH)_2$ catalyst with adjustable oxygen vacancies is synthesized through electrodeposition from an 1ChCl–2EG DES solution containing $Ni(NO_3)_2$ and NaH_2PO_2. Introducing water into the DES adjusts the hydrogen bonding between ChCl and EG, thus enhancing electrical conductivity and control over oxygen vacancies.[149]

4.5 Strong coatings with organic and inorganic additives

In electrodeposition, incorporating organic compounds and inorganic salts is essential for improving the mechanical properties of metal coatings. These additives enhance smoothness and hardness and affect the growth and heteroatom doping within the coatings.

Hasan et al. used 1ChCl–2EG DES to dissolve $ZnCl_2$ with additives such as nicotinic acid (NA), boric acid, and benzoquinone for zinc electrodeposition. These additives, serving as brighteners, refined the smoothness and fineness of the zinc deposits. However, boric acid and benzoquinone adsorb on the cathodic electrode, inhibiting zinc nuclei growth and reducing film thickness. Typically, zinc grows along the (002), (101), and (102) planes, but NA and boric acid redirect their growth to the (100), (101), and (110) planes.[150] Using a method involving supercritical carbon dioxide (SC-CO_2)-assisted electrodeposition from 1ChCl–urea DES with $ZnCl_2$ and additives like threonine (Thr) or a NA/ascorbic acid (AA) mixture, the hardness of Zn coatings improved by 30% compared to conventional methods (Fig. 11A). This approach also altered the crystal structure, eliminating the hexagonal closest-packed zinc (100) diffraction peak and reducing grain size and hydrogen bubble formation, thus smoothing the cathode surface.[151] Additionally, introducing 0.06 M NA during ZnO_2 electrodeposition transformed the zinc morphology, significantly enhancing surface density and smoothness.[152]

Inorganic salts also significantly enhance the performance of electrodeposited coatings. For example, Ag is electrodeposited from 1ChCl–2EG DES electrolyte containing AgCl and KBr,
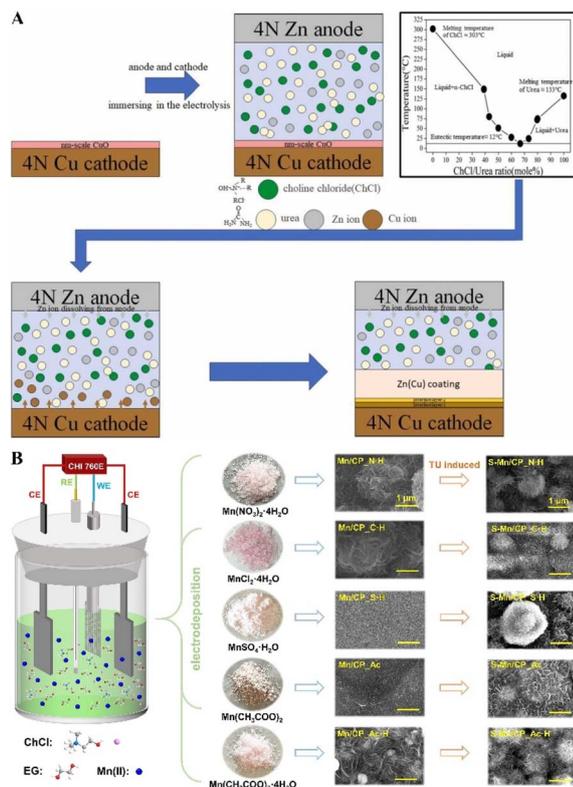
Fig. 11 Fabrication of coatings through the DES electrodeposition process with additives. (A) Process outline for using $SC-CO_2$-assisted electrodeposition to synthesize Zn coatings. Reprinted with permission from copyright© Elsevier Ltd, 2023.[151]. (B) Schematic diagram of Mn/CP and S-Mn/CP electrodes electrodeposited from 1ChCl–2EG DES containing different anions. Reprinted with permission from copyright© Elsevier B. V., 2023.[155]

which negatively shifts the reduction peak potential of Ag^+, resulting in denser coatings and a preferred orientation on the Ag (111) crystal plane.[153] Similarly, a mixture of boric acid and $CuSO_4 \cdot 5H_2O$ in 1ChCl–2EG DES produces a mirror-like nickel surface with improved quality and reduced roughness. The presence of Cu^{2+} in the DES enhances nickel electrodeposition uniformity.[154] During the electrodeposition of S-doped Mn on carbon paper (S-Mn/CP) in 1ChCl–2EG DES containing various manganese salts and thiourea, nitrate anions and crystal water facilitate the formation of manganese oxide/hydroxide (Fig. 11B). In contrast, sulfate anions remain stable and do not participate in the reaction. The introduction of crystal water and thiourea partially replace chlorine in manganese complexes, forming $[Mn(Cl)_{6-x}(H_2O)_x]_{x-4}$ and $[Mn(Cl)_{6-x-y}(TU)_y(H_2O)_x]_{x+y-4}$ complexes, which accelerate the electrodeposition process.[155]

This chapter delves into the electrodeposition of alloys, metal oxides, phosphides, hydroxides, carbon materials, and polymers using DESs. These solvents serve as a versatile medium for tailoring the properties of materials. The process exploits the unique electrochemical properties of DESs to control the synthesis of materials with precision, optimizing the deposition dynamics. Researchers utilize DESs to enhance

materials' structural and functional attributes, often surpassing traditional methods' capabilities. Additionally, incorporating organic compounds or inorganic salts into DESs modulates nucleation and growth, aiding in grain refinement, surface tension adjustment, doping, and inhibitory effects. Consequently, electrodeposition in DESs facilitates the meticulous design of materials with bespoke properties, fostering innovative techniques and furthering advancements in materials science.

5 Outlook and summary

Deep Eutectic Solvents (DESs) have emerged as a promising class of green solvents with significant potential for material synthesis applications. These solvents serve as media and actively participate in the formation and structural regulation of materials, introducing innovative dimensions to materials science research. DESs outperform their pure components in material fabrication by offering enhanced solubility, improved reaction control, and superior material properties, while also being more sustainable and cost-effective. These advantages make DESs a promising choice for the development of advanced materials across various applications. It is crucial for future research to explore the potential, challenges, and innovations of DESs from diverse perspectives.

Firstly, DESs offer unique synthesis capabilities that provide extensive opportunities for developing new materials through solvothermal synthesis, annealing, microwave synthesis, precipitation, and electrodeposition. Although known for their multifunctionality and environmental benefits, further research is necessary to understand their adaptability and selectivity across various material systems.

Secondly, understanding the interaction between DESs and materials' structural and functional properties is essential. The influence of DESs' molecular structure and composition on material synthesis remains under-explored, particularly in complex multi-component systems. Future studies should aim to elucidate the microscopic reaction mechanisms of DESs and their impact on the resulting materials' crystal structure, morphology, and properties, enabling precise control over material synthesis and the development of high-performance materials.

Thirdly, the role of DESs in material functionalization is receiving increasing attention. As modifiers, DESs can influence the surface properties of materials, impacting their performance in catalysis and energy storage. Current research is often limited to specific instances, and systematic studies are needed to understand the surface modification effects of DESs across different material systems and their overall impact, which could lead to the development of novel functional materials and broaden the applications of DESs.

Fourthly, the advantages of DESs make them promising for green chemistry applications, but their potential limitations highlight the need for further research. Efforts to lower viscosity, such as the incorporation of co-solvents, may mitigate some drawbacks but require careful evaluation to avoid compromising their environmental benefits. Similarly,

expanding our understanding of DES stability and environmental impact will be critical for their wider adoption. While DESs represent a significant step forward in sustainable solvent technology, their current drawbacks necessitate targeted innovations to optimize their performance and broaden their industrial applicability.

Finally, the potential of DESs in emerging fields such as energy storage, environmental remediation, and biomaterials is only beginning to be realized. Future research should focus on developing innovative functional materials based on DESs and evaluating their practical applications. As knowledge of DESs expands, more potential applications may emerge, advancing the field of materials science.

In conclusion, DESs are poised to influence the future of material synthesis significantly. Although substantial progress has been achieved, many challenges must be addressed. It is crucial to investigate the applications of DESs across various synthesis methods, elucidating their mechanisms of action and enhancing their industrial applications. These efforts will establish DESs as a critical tool in advancing materials science. Future research is anticipated to produce transformative outcomes, driving the development of DESs within materials science and engineering.

Data availability

The data that support the findings of this study are available in the request from the corresponding author (jiangjingyun@zzu.edu.cn) upon reasonable request.

Conflicts of interest

There are no conflicts to declare.

Acknowledgements

References

1 N. Winterton, *Clean Technol. Environ. Policy*, 2021, **23**, 2499–2522.

2 C. J. Clarke, W.-C. Tu, O. Levers, A. Brohl and J. P. Hallett, *Chem. Rev.*, 2018, **118**, 747–800.

3 G. Kaur, H. Kumar and M. Singla, *J. Mol. Liq.*, 2022, **351**, 118556.

4 S. S. de Jesus and R. Maciel Filho, *Renewable Sustainable Energy Rev.*, 2022, **157**, 112039.

5 F. M. Perna, P. Vitale and V. Capriati, *Curr. Opin. Green Sustainable Chem.*, 2020, **21**, 27–33.

6 S. P. Ijardar, V. Singh and R. L. Gardas, *Molecules*, 2022, **27**, 1368.

7 S. Azmi, M. F. Koudahi and E. Frackowiak, *Energy Environ. Sci.*, 2022, **15**, 1156–1171.

8 A. P. Abbott, G. Capper, D. L. Davies, R. K. Rasheed and V. Tambyrajah, *Chem. Commun.*, 2003, **1**, 70–71.

9 C. Florindo, F. S. Oliveira, L. P. N. Rebelo, A. M. Fernandes and I. M. Marrucho, *ACS Sustain. Chem. Eng.*, 2014, **2**, 2416–2425.

10 E. L. Smith, A. P. Abbott and K. S. Ryder, *Chem. Rev.*, 2014, **114**, 11060–11082.

11 D. O. Abranches, M. A. Martins, L. P. Silva, N. Schaeffer, S. P. Pinho and J. A. Coutinho, *Chem. Commun.*, 2019, **55**, 10253–10256.

12 B. B. Hansen, S. Spittle, B. Chen, D. Poe, Y. Zhang, J. M. Klein, A. Horton, L. Adhikari, T. Zelovich and B. W. Doherty, *Chem. Rev.*, 2020, **121**, 1232–1285.

13 Y. Ma, Y. Yang, T. Li, S. Hussain and M. Zhu, *Green Chem.*, 2024, **26**, 3627–3669.

14 R. Deng, M. Gao, B. Zhang and Q. Zhang, *Adv. Energy Mater.*, 2024, **14**, 2303707.

15 D. Yu, Z. Xue and T. Mu, *Cell Rep. Phys. Sci.*, 2022, **3**, 100809.

16 N. N. Nam, H. D. K. Do, K. T. L. Trinh and N. Y. Lee, *Nanomaterials*, 2023, **13**, 1164.

17 M. Teixeira, R. A. Maia, L. Karmazin, B. Louis and S. A. Baudron, *CrystEngComm*, 2022, **24**, 601–608.

18 R. A. Maia, B. Louis and S. A. Baudron, *Dalton Trans.*, 2021, **50**, 4145–4151.

19 R. A. Maia, A. Fluck, C. Maxim, B. Louis and S. A. Baudron, *Green Chem.*, 2023, **25**, 9103–9108.

20 X. Wang, L. Wang, K. K. Rani, X. Peng, Y. Ning, X. Liu, Y. Fan, D.-H. Chen and W. Chen, *Inorg. Chem. Front.*, 2023, **11**, 98–106.

21 H. Ren, Y. Liu, R. Zhang, Y. Zheng, T. Zhao, J. Han, C. Chen and E. Duan, *J. Environ. Chem. Eng.*, 2023, **11**, 109988.

22 R. Zhang, Y. Zheng, Q. Zhang, Z. Wu, L. Wang, J. Zhang, H. Ren and E. Duan, *J. Environ. Chem. Eng.*, 2024, **12**, 112391.

23 M. Tian, D. Wang, Q. Liu, L. Wang, Y. Tao, J. Wang, Y. Zou, Y. Yang, Q. Zhou, L. Li, M. Wang, X. Li and D. Gao, *J. Mol. Liq.*, 2024, **397**, 112391.

24 G. Fu, C. Gao, K. Quan, H. Li, H. Qiu and J. Chen, *Anal. Bioanal. Chem.*, 2023, **415**, 4255–4264.

25 P. Lai, H. Zhou, Z. Niu, L. Li, W. Zhu and L. Dai, *Chem. Eng. J.*, 2023, **457**, 141255.

26 S. Chinnapaiyan, H. T. Das, S.-M. Chen, M. Govindasamy, R. A. Alshgari, C.-H. Fan and C.-H. Huang, *J. Alloys Compd.*, 2023, **931**, 167553.

27 X. Liu, C. Huang, M. Waqas, L. Wang, D. Huang, Q. Huang, Z. Yang, Y. Fan, C. Hou and W. Chen, *Mol. Catal.*, 2023, **551**, 113612.

28 R. Wang, X. Ma, D. Ding, B. Huang, Z. Zhu, T. Su, W. Liao, H. Lue and K. Yang, *Inorg. Chem. Front.*, 2023, **10**, 5420–5429.

29 S. K. Shahi, S. Sandhu, N. Kaur, J. S. Shahi, M. Kaur, V. Singh and V. Singh, *New J. Chem.*, 2022, **46**, 18865–18873.

30 G. Yao, N. Zhang, Y. Zhang and T. Zhou, *J. Alloys Compd.*, 2022, **892**, 162205.

31 M. M. Stanley, V. A. Sherlin, S.-F. Wang, B. Sriram, J. N. Baby and M. George, *J. Environ. Chem. Eng.*, 2023, **11**, 110185.

32 S. Liu, B. Zhang, Z. Yang, Z. Xue and T. Mu, *Green Chem.*, 2023, **25**, 2620–2628.

33 H. Zhao, W. Li and R. Wang, *Mater. Adv.*, 2022, **3**, 7125–7131.

34 T. Zhang, T. Doert and M. Ruck, *Z. Anorg. Allg. Chem.*, 2017, **643**, 1913–1919.

35 B. Mahto, A. A. Khan, A. Barhoi and S. Hussain, *ACS Appl. Nano Mater.*, 2023, **6**, 6784–6797.

36 T. Kokulnathan, T.-J. Wang, F. Ahmed and S. Kumar, *J. Mol. Liq.*, 2023, **369**, 120785.

37 H. Yang, Z. Cheng, P. Wu, Y. Wei, J. Jiang and Q. Xu, *Electrochim. Acta*, 2022, **427**, 140879.

38 W. Chen, X. Bai, Z. Xue, H. Mou, J. Chen, Z. Liu and T. Mu, *New J. Chem.*, 2019, **43**, 8804–8810.

39 Z. Cheng, H. Yang, Y. Xu, J. Jiang and Q. Xu, *Mater. Today Chem.*, 2022, **26**, 101214.

40 H. Zhang, Y. Zhao, Z. Cheng, J. Jiang, J. Fu and Q. Xu, *Small*, 2024, **20**(47), 2405225.

41 Y. Xu, Z. Cheng, J. Jiang, J. Du and Q. Xu, *Chem. Commun.*, 2021, **57**, 13170–13173.

42 Y. Wei, Y. Xu, H. Zhang, J. Jiang and Q. Xu, *New J. Chem.*, 2024, **48**, 11206–11210.

43 J. Jiang, P. Yan, Y. Zhou, Z. Cheng, X. Cui, Y. Ge and Q. Xu, *Adv. Energy Mater.*, 2020, **10**, 2002214.

44 X. Su, X. Shao, Y. Wang, W. Fan, C. Song and D. Wang, *ACS Appl. Nano Mater.*, 2023, **6**, 23029–23036.

45 R. Xue, R. Deng, Y. Li, M. Gao, J. Wang and Q. Zhang, *Green Chemical Engineering*, 2024, **6**(1), 93–101.

46 K. Zou, Z. Guan, Y. Deng and G. Chen, *Carbon*, 2020, **161**, 25–35.

47 D. Zhang, X. Zhan, T. Zhou, J. Du, K. Zou and Y. Luo, *J. Mater. Sci. Technol.*, 2024, **193**, 22–28.

48 R. Huang, A. Zhong, K. Huang, Y. Yu, Y. Tang and P. Xia, *J. Environ. Chem. Eng.*, 2023, **11**, 111474.

49 D. Aydemir, M. E. Ergun, S. K. Gulsoy, Z. E. Ozan and G. Gunduz, *Biofuels Bioproducts & Biorefining-Biofpr*, 2024, **18**, 251–264.

50 M. Xu, X. Zhu, Y. Lai, A. Xia, Y. Huang, X. Zhu and Q. Liao, *Appl. Energy*, 2024, **353**, 122095.

51 Q. Liu, T. Wang, C. Wang and D. Wu, *Chem. Eng. J.*, 2024, **481**, 148292.

52 C. Wang, T. Wang, Q. Liu and D. Wu, *Fuel*, 2024, **362**, 115965.

53 C. O. Ehi-Eromosele, C. N. Onwucha, S. O. Ajayi, G. Melinte, A.-L. Hansen, S. Indris and H. Ehrenberg, *RSC Adv.*, 2022, **12**, 34670–34684.

54 R. Zhou, C. Xu, J. Yang, D. Guan and J. Cai, *Chem. Lett.*, 2020, **49**, 585–588.

55 D. Li, Y. Huang, Z. Li, L. Zhong, C. Liu and X. Peng, *Chem. Eng. J.*, 2022, **430**, 132783.

56 D. Zhang, C. Sun, D. Liu, C. Song and D. Wang, *Sci. China Mater.*, 2023, **66**, 1362–1372.

57 H. Mou, J. Wang, D. Zhang, D. Yu, W. Chen, D. Wang and T. Mu, *J. Mater. Chem. A*, 2019, **7**, 5719–5725.

58 M. M. Stanley, V. A. Sherlin, S.-F. Wang, J. N. Baby, B. Sriram and M. George, *J. Mol. Liq.*, 2023, **375**, 121308.

59 P. Yang, X. Wei, L. Zhang, S. Dong, W. Cao, D. Ma and Y. Ouyang, *Molecules*, 2023, **28**, 2995.

60 H. Li, S. Xu, H. Qi, X. Cao, D. Ju, C. Chen, Y. Chen, S. Li and L. Chang, *Energy Technol.*, 2023, **11**, 2201400.

61 S. Xu, X. Cao, F. Li, H. Li, H. Qi, J. Zhang, C. Chen and D. Ju, *J. Alloys Compd.*, 2023, **936**, 168080.

62 M. Zhang, X. Wu, X. Liu, H. Li, Y. Wang and D. Wang, *Molecules*, 2023, **28**, 7878.

63 Y. Li, Y. Bao, B. Han, Y. Zhuang, H. Li, C. Chen and D. Ju, *Flatchem*, 2024, **45**, 100635.

64 Y. Zhang, Z. Xue, X. Zhao, B. Zhang and T. Mu, *Green Chem.*, 2022, **24**, 1721–1731.

65 M. Iwanow, J. Seidler, L. Vieira, M. Kaiser, D. Van Opdenbosch, C. Zollfrank, T. Gaertner, M. Richter, B. Koenig and V. Sieber, *Catalysts*, 2021, **11**, 542.

66 S. Zhang, M. Sun, K.-Y. Wang, L. Cheng, S. Zhang and C. Wang, *ACS Sustain. Chem. Eng.*, 2021, **9**, 2358–2366.

67 H. Ying, T. Chen, C. Zhang, J. Bi, Z. Li and J. Hao, *J. Colloid Interface Sci.*, 2021, **602**, 64–72.

68 A. Soeldner, J. Zach, M. Iwanow, T. Gaertner, M. Schlosser, A. Pfitzner and B. Koenig, *Chem.–Eur. J.*, 2016, **22**, 13108–13113.

69 S. Hong, R. M. Doughty, F. E. Osterloh and J. V. Zaikina, *J. Mater. Chem. A*, 2019, **7**, 12303–12316.

70 B. He, Y. Li, T. Zhang, Y. Shi, K. Li, F. Dai, R. Zhang, R. Liu and S. Zhang, *J. Phys. Chem. B*, 2020, **124**, 3743–3753.

71 S. Sandhu, M. Kaur, N. Sharma, N. Kaur and V. Singh, *Catal. Sci. Technol.*, 2022, **12**, 6717–6727.

72 W. Song, C. Liu, J. Yan, L. Zhou and L. Zhang, *J. Photochem. Photobiol., A*, 2024, **451**, 115482.

73 D. P. Jaihindh, P. Anand, R.-S. Chen, W.-Y. Yu, M.-S. Wong and Y.-P. Fu, *J. Environ. Chem. Eng.*, 2023, **11**, 109852.

74 Y. Wang, K. Rong, J. Wei, S. Chang, D. Yu, Y. Fang and S. Dong, *Nano Res.*, 2023, **16**, 11430–11443.

75 J. Wei, K. Rong, Y. Wang, L. Liu, Y. Fang and S. Dong, *Nano Res.*, 2023, **16**, 10381–10391.

76 E. J. Luke, J. Potticary, S. Friedemann and S. R. Hall, *Dalton Trans.*, 2023, **52**, 3188–3194.

77 S. Hong, A. M. Diez, A. N. Adeyemi, J. P. S. Sousa, L. M. Salonen, O. I. Lebedev, Y. V. Kolen'ko and J. V. Zaikina, *ACS Appl. Mater. Interfaces*, 2022, **14**, 23277–23284.

78 I. Manasi, M. R. Andalibi, R. Castaing, L. Torrente-Murciano and K. J. Edler, *J. Mater. Chem. A*, 2022, **10**, 18422–18430.

79 X.-y. Liu, X.-p. Li, R.-x. Zhao and H. Zhang, *New J. Chem.*, 2021, **45**, 15901–15911.

80 S. Guan, B. Xu, J. Wu, J. Han, T. Guan, Y. Yang, K. Li and J. Wang, *Fuel*, 2024, **358**, 130315.

81 M. Bao, S. Chen, X. Shao, H. Deng, A. Mao and J. Tan, *Chin. J. Chem.*, 2024, **82**, 303–313.

82 J. Wei, K. Rong, X. Li, Y. Wang, Z.-A. Qiao, Y. Fang and S. Dong, *Nano Res.*, 2022, **15**, 2756–2763.

83 C. Lai, K. Chen, M. Lei, J. Hu, S. Chen and C. Li, *Adv. Funct. Mater.*, 2024, **34**, 2312415.

84 C. Lai, K. Chen, Y. Zheng, J. Meng, J. Hu and C. Li, *J. Energy Chem.*, 2023, **78**, 178–187.

85 J. Jiang, L. Chang, W. Zhao, Q. Tian and Q. Xu, *Chem. Commun.*, 2019, **55**, 10174–10177.

86 Y. Wei, J. Jiang, J. Dong, Y. Xu, J. Fu and Q. Xu, *Green Chem.*, 2022, **24**, 8014–8020.

87 R. Tabaraki and F. Nazari, *J. Photochem. Photobiol., A*, 2023, **444**, 114891.

88 H. Kaur, M. Singh, K. Singh, A. Kumar and T. S. Kang, *Green Chem.*, 2023, **25**, 5172–5181.

89 Y. Xie, J. Zhao, P. Wang, Z. Ji, Z. Ling and Q. Yong, *Ind. Crops Prod.*, 2023, **191**, 115965.

90 A. N. Adeyemi, R. A. Earnest, T. Cox, O. I. Lebedev and J. V. Zaikina, *Molecules*, 2022, **27**, 1815.

91 A. N. Adeyemi, M. Clemente, S. J. Lee, A. Mantravadi and J. V. Zaikina, *ACS Appl. Energy Mater.*, 2022, **5**, 14858–14868.

92 L. Deng, L. Wang, S. Liu, Q. Liu, J. Wang, Y. Tao, M. Tian, Y. Yang, Y. Zou, H. Niu, D. Wang and D. Gao, *Macromolecules*, 2023, **56**, 7707–7720.

93 J. Qiu, P. Guan, Y. Zhao, Z. Li, H. Wang and J. Wang, *Green Chem.*, 2020, **22**, 7537–7542.

94 S. Wei, H. Li, K. Li, R. Zhang, G. Wang and R. Liu, *Ind. Eng. Chem. Res.*, 2022, **61**, 17842–17853.

95 Y. H. Kim, J.-H. Oh and J.-S. Lee, *J. Ind. Eng. Chem.*, 2022, **112**, 182–192.

96 B. Li, H. Zhang, J. Kaelin, S. Gao, F. Xia, B. An, K. Lu and Y. Cheng, *ACS Appl. Nano Mater.*, 2023, **6**, 3184–3190.

97 H. Wagata, G. Harada, E. Nakashima, M. Asaga, T. Watanabe, Y. Tanaka, M. Tada and K. Yubuta, *Crystengcomm*, 2021, **23**, 8367–8378.

98 H. Jabeen, S. Shaukat and H. M. A. U. Rahman, *J. Mol. Liq.*, 2024, **395**, 123783.

99 R. Balaji and D. Ilangeswaran, *Mater. Today: Proc.*, 2022, **56**, 3366–3375.

100 Y. Zhang, J. Ru, P. Huang, Y. Jiang and E. Wu, *Adv. Powder Technol.*, 2023, **34**, 104200.

101 C. Thanh Phuong, H. Chuc Nguyen, V.-Q. Hieu, D. M. Kabtamu, S. Kumar, N. Van Cuong and C. Xuan Thang, *New J. Chem.*, 2022, **46**, 3786–3793.

102 Q. Lu, H. Li and Z. Tan, *ACS Appl. Mater. Interfaces*, 2023, **15**, 34055–34063.

103 K. Aruchamy, N. Maalige, M. M. Halanur, A. Mahto, R. Nagaraj, D. Kalpana, D. Ghosh, D. Mondal and S. Kotrappanavar Nataraj, *Chem. Eng. J.*, 2020, **379**, 122327.

104 X. Peng, P. Liu, T. Zeng, H. Cui, M. Wang, J. Li, K. Liu, Q. Wang and Y. Liu, *J. Sol-Gel Sci. Technol.*, 2024, **109**, 695–706.

105 H. Chen, W. Jiang, N. Zhao, X. Zhang, X. Ma, H. Jia, Y. Zhuang and M. Guan, *New J. Chem.*, 2023, **47**, 7903–7909.

106 L. Gontrani, D. T. Donia, E. M. Bauer, P. Tagliatesta and M. Carbone, *Inorg. Chim. Acta*, 2023, **545**, 121268.

107 A. Samage, K. Pramoda, M. Halakarni and N. S. Kotrappanavar, *ACS Appl. Energy Mater.*, 2023, **6**, 2412–2422.

108 Y. Liu, X. Yang, J. Hu, N. Lu, D. He, H. Chi, Y. Liu, S. Yang and X. Wen, *Anal. Chim. Acta*, 2024, **1290**, 342197.

109 N. Noorani and A. Mehrdad, *Sci. Rep.*, 2023, **13**, 13012.

110 X. Wang, Y. Wang, Y. Kang, B. Yao and X. Peng, *Nanoscale*, 2023, **15**, 15626–15634.

111 J. Ye, Y. Gao, Q. Xu, Z. Jin, G. Wu, S. Wang, Z. Cai, K. Yang, Q. Wu and Q. Li, *Chem. Eng. J.*, 2023, **477**, 147142.

112 L. M. Murillo-Herrera, E. S. Aguilar, M. W. Thielke and A. Jorge Sobrido, *Chem.–Asian J.*, 2023, **18**, e202201208.

113 L. Valentino, R. Di Forti, A. Morena, C. Aprile, M. Gruttadauria, F. Giacalone and V. Campisciano, *Chem. Eng. J.*, 2024, **489**, 151447.

114 T. Ahmad, J. Iqbal, M. A. Bustam, M. Babar, M. B. Tahir, M. Sagir, M. Irfan, H. M. A. Asghar, A. Hassan, A. Riaz, L. F. Chuah, A. Bokhari, M. Mubashir and P. L. Show, *Environ. Res.*, 2023, **222**, 115314.

115 Q. Zheng, Y. Zhou, J. Huang, H. Lu, S. Wu, J. Zhang, Y. Li, W. Hong, X. Tan, J. Lin, Q. Chen, F. Li, Z. Cai and M. Zhang, *J. Alloys Compd.*, 2024, **986**, 174155.

116 A. Bazzaz Dilmaghani, M. R. Afshar Mogaddam, F. Monajjemzadeh and M. A. Farajzadeh, *Anal. Sci.*, 2022, **39**, 169–178.

117 V. Sales, C. Paternoster, D. Mantovani and G. Kolliopoulos, *Journal of Ionic Liquids*, 2024, **4**, 100086.

118 L. P. M. dos Santos, R. M. Freire, S. Michea, J. C. Denardin, D. B. Araujo, E. B. Barros, A. N. Correia and P. De Lima-Neto, *J. Mol. Liq.*, 2019, **288**, 111038.

119 V. A. Medina, M. G. M. de Oca, J. I. Aldana, M. A. Romero and M. E. Palomar, *ECS Trans.*, 2023, **110**, 103.

120 F. Liu, C. Chen, X. Jiang, J.-Y. Guo, Y. Wei, J.-W. Li, T. Sheng, X. Zhao and L. Wei, *ACS Sustain. Chem. Eng.*, 2023, **11**, 1631–1637.

121 Y.-J. Mao, F. Liu, Y.-H. Chen, X. Jiang, X.-S. Zhao, T. Sheng, J.-Y. Ye, H.-G. Liao, L. Wei and S.-G. Sun, *J. Mater. Chem. A*, 2021, **9**, 26277–26285.

122 P. M. Viyanni, T. N. J. I. Edison and M. G. Sethuraman, *Materials Today Sustainability*, 2023, **24**, 100565.

123 Y.-H. Liu, H.-W. Guo and F.-Y. Zeng, *J. Power Sources*, 2023, **570**, 233043.

124 W.-F. Kuan, C.-L. Chen, M. S. Ahmad, C.-H. Hsieh, H. M. Chen and J. F. Su, *Adv. Sustainable Syst.*, 2024, **8**, 2300425.

125 D. N. Rodrigues-Junior, N. G. Sousa, F. M. T. Luna, T. M. B. F. Oliveira, D. S. Abreu, W. Schwarzacher, P. de Lima-Neto and A. N. Correia, *J. Electroanal. Chem.*, 2023, **947**, 117785.

126 J. C. Pereira, L. P. M. dos Santos, A. A. C. Alcanfor, O. S. Campos, P. N. S. Casciano, A. N. Correia and P. de Lima-Neto, *Electrochim. Acta*, 2022, **407**, 139647.

127 B. Li, C. Zheng, C. Pan, F. Pan, T. Lv, X. Wang, X. Ju, K. Gong, W. Zou and G. Yi, *Mater. Chem. Phys.*, 2024, **317**, 129071.

128 C.-W. Lin, Y.-H. Chen, P.-C. Chou and Y.-T. Hsieh, *Microchem. J.*, 2024, **200**, 110328.

129 C. Chen, J. Guo, J. Liu, W. Li, Y. Wei, H. Wang, X. Zhao and L. Wei, *Chem. Commun.*, 2023, **59**, 12863–12866.

130 Y.-c. Xu, W.-j. Chen, J.-f. Zhou, C.-b. Hu, S.-w. He, H. Liu and Z.-s. Hua, *Langmuir*, 2024, **40**, 14291–14302.

131 W. Liu, W. Li, W. Dong, L. Guo, Y. Zou, C. Yu, C. Sun, N. Huang and X. Sun, *J. Power Sources*, 2024, **606**, 234518.

132 S. Costovici, A. Pantazi, D. Balan, A. Cojocaru, T. Visan, M. Enachescu and L. Anicai, *Metals*, 2023, **13**, 203.

133 A. T. S. C. Brandão, S. Rosoiu, R. Costa, O. A. Lazar, A. F. Silva, L. Anicai, C. M. Pereira and M. Enachescu, *J. Mater. Res. Technol.*, 2021, **15**, 342–359.

134 Z. Zhang, Z. Wang, Y. Sun, S. Jiang, L. Shi, Q. Bi and J. Xue, *J. Electroanal. Chem.*, 2022, **911**, 116225.

135 X. Lai, Z. Dang, L. Wang, P. Li, Y. Yang and C. Wang, *J. Energy Storage*, 2024, **91**, 112032.

136 I. B. Qader, H. K. Ismail, H. F. Alesary, J. H. Kareem, Y. T. Maaroof and S. Barton, *J. Electroanal. Chem.*, 2023, **951**, 117943.

137 M. E. Voicu, F. Golgovici, M. Prodana, D. Draganescu and I. Demetrescu, *Materials*, 2023, **16**, 4387.

138 Y. H. Chang, P. M. Woi and Y. B. Alias, *Electrocatalysis*, 2021, **12**, 238–250.

139 T. Atici, M. B. Kamac, M. Yilmaz and A. Y. Kabaca, *Electrochim. Acta*, 2023, **458**, 142484.

140 W. da Silva, A. C. Queiroz and C. M. A. Brett, *Electrochim. Acta*, 2020, **347**, 136284.

141 R. M. Buoro, J. M. S. Almeida and C. M. A. Brett, *Electrochim. Acta*, 2024, **490**, 144305.

142 M. Ding, T. Hou, H. Niu, N. Zhang, P. Guan and X. Hu, *J. Electroanal. Chem.*, 2022, **920**, 116602.

143 X. Liang, Y. Zhou, J. M. S. Almeida and C. M. A. Brett, *J. Electroanal. Chem.*, 2023, **936**, 117366.

144 J. M. S. Almeida, Z. S. B. Pedro, R. M. Buoro and C. M. A. Brett, *Chem.–Eur. J.*, 2024, **30**(58), e202401752.

145 H. Jia, J. Sun, M. Dong, H. Dong, H. Zhang and X. Xie, *Nanoscale*, 2021, **13**, 19004–19011.

146 H. Jia, F. Zhang, J. Sun, S. Jiang, Q. Yin, Y. Zhang and X. Xie, *Colloids Surf., A*, 2023, **660**, 130864.

147 Y. Wu, Z. Zhou, Q. Yao, J. Wang, Y. Tian, S. Liu and C. Wang, *J. Alloys Compd.*, 2023, **942**, 169070.

148 Y. Hu, W. Li, L. Li, J. Wu, S. Sheng and H. Wang, *Appl. Catal., A*, 2023, **662**, 119267.

149 Q. Li, M. Gao, M. Cheng, H. Li, Y. Hua, Q. Zhang and J. Ru, *Electrochim. Acta*, 2024, **478**, 143859.

150 H. F. Alesary, S. Cihangir, A. D. Ballantyne, R. C. Harris, D. P. Weston, A. P. Abbott and K. S. Ryder, *Electrochim. Acta*, 2019, **304**, 118–130.

151 C.-Y. Lee, W.-Y. Chen, J.-K. Chang and H.-B. Lee, *Mater. Today Commun.*, 2024, **38**, 107941.

152 S. Xu, F. Li, C. Chen, N. Bai, D. Ju, J. Zhang and X. Li, *J. Mol. Liq.*, 2024, **397**, 124094.

153 C. Zhan, R. Zhang, X. Fu, H. Sun, X. Zhou, B. Wang, H. Li and J. Sun, *Ionics*, 2023, **29**, 4325–4335.

154 G. Qadr, M. I. Awad, K. Haji, J. A. Jumaa and H. H. Abdallah, *J. Mol. Liq.*, 2023, **378**, 121584.

155 M. Guo, B. Zhang and Q. Zhang, *Appl. Surf. Sci.*, 2024, **645**, 158843.